

# Finte-size induced random switching of chimeras in a deterministic two-population Kuramoto-Sakaguchi model

Henry Irvine<sup>1, a)</sup> and Georg A. Gottwald<sup>1, b)</sup>

*School of Mathematics and Statistics, The University of Sydney, Sydney, NSW 2006, Australia*

The two-population Kuramoto-Sakaguchi model for interacting populations of phase oscillators exhibits chimera states whereby one population is synchronised and the other is desynchronised. Which of the two populations is synchronised depends on the initial conditions. We show that this deterministic model exhibits random switches of their chimera states, alternating between which of the two populations is synchronised and which is not. We show that these random switches are induced by the finite size of the network. We provide numerical evidence that the switches are governed by a Poisson process and that the time between switches grows exponentially with the system size, rendering switches unobservable for all practical purposes in sufficiently large networks. We develop a reduced stochastic model for the synchronised population, based on a central limit theorem controlling the collective effect of the desynchronised population on the synchronised one, and show that this stochastic model well reproduces the statistical behaviour of the full deterministic model. We further determine critical fluctuation sizes capable of inducing switches and provide estimates for the mean switching times from an associated Kramers problem.

## I. INTRODUCTION

Coupled oscillators describe systems ranging from neurons in the brain<sup>1–3</sup> and synchronous firefly flashing<sup>4</sup>, to power grids<sup>5,6</sup> and Josephson junction arrays<sup>7,8</sup>. The celebrated Kuramoto model and its numerous variants<sup>9–17</sup> constitutes a paradigmatic model to describe the temporal evolution of such coupled oscillators and its often rich dynamical behaviour. Much progress has been made by employing mean-field theory, valid in the thermodynamic limit of infinitely many oscillators<sup>10,18,19</sup>. However, recently a number of finite-size effects have attracted attention such as finite-size induced stochastic drifts of oscillators which disappear in the thermodynamic limit<sup>20–23</sup>. Such finite-size effects are not amenable to the classical mean-field theory and require new analytical approaches<sup>20–27</sup>.

We present a dynamical phenomenon which is due entirely to the finite size of the number of oscillators. We describe the emergence of a stochastic switching of chimera states in a deterministic system of a two-population Kuramoto-Sakaguchi (KS) model<sup>28,29</sup>. Chimeras denote a symmetry breaking state in which a group of oscillators is synchronised while the rest of the oscillators are desynchronised and where the partition into a synchronised and desynchronised group depends on the initial condition<sup>30–33</sup>. The existence of chimera states in a two-population KS model is well known and has been studied in either small networks<sup>34,35</sup> or in the thermodynamic limit<sup>36–38</sup>. Chimeras can undergo complex dynamical behaviour. In switching (or alternating) chimeras the synchronised and desynchronised regions alternate in time. To date such switching has been attributed to either the existence of metastable states<sup>39–43</sup>

or to heteroclinic cycles<sup>44–50</sup>. We report here on the effective stochastic behaviour of switching between a synchronised population and a desynchronised population in a deterministic two-population KS model, where the switching is mediated entirely by finite-size effects and disappears in sufficiently large networks. Numerical simulations will show that the mean switching time increases exponentially with the number of oscillators  $N$  and that the variance of the order parameter scales as  $1/N$ , suggesting an underlying central limit theorem which captures fluctuations around the well-known deterministic thermodynamic limit. We will describe the fluctuations by means of the recently proposed stochastic model reduction for deterministic KS models<sup>51</sup>. We adopt the stochastic modelling framework to parametrise the interaction term that couples the phases of the desynchronised population to those of the synchronised one by a Gaussian process. Gaussian processes are entirely determined by their mean and their covariance function. The mean, represented by the thermodynamic limit of infinitely many oscillators, can be estimated by classical mean field theory. The covariance function will be estimated by first approximating the Gaussian process by a complex Ornstein-Uhlenbeck process, and then numerically determining the parameters of this complex Ornstein-Uhlenbeck process to fit the observed covariance function of the finite-size fluctuations. This modelling strategy captures the statistical features of the full two-population KS model very well, including the distribution of the order parameter. We will further determine the critical fluctuation size which is sufficient to induce chimera switching, and set up a classical Kramers problem to approximate the mean switching time with reasonable accuracy<sup>52</sup>. Our modelling strategy requires the system size to be sufficiently large to allow for the underlying central limit theorem to be valid and sufficiently small to prevent the law of large numbers described by the thermodynamic limit and classical mean-field theory.

The paper is organised as follows. Section II presents

<sup>a)</sup>Electronic mail: hirv6523@uni.sydney.edu.au

<sup>b)</sup>Electronic mail: georg.gottwald@sydney.edu.au

the deterministic two-population KS model. Section II A reviews the mean-field theory. Section III presents results of numerical simulations of the two-population KS model showing that switches of the chimera states occur in an effective stochastic way in finite-size networks. Section IV presents a deterministic model reduction which will inform the estimation of the mean switching time. Section V presents the stochastic model reduction for a synchronised population. Section VI provides results of numerical simulations showing that the reduced stochastic model well captures the dynamics of the full system and quantitatively describes the statistics of the observed random switching of chimeras. We conclude with a discussion and an outlook in Section VII.

## II. KURAMOTO-SAKAGUCHI MODEL FOR TWO INTERACTING POPULATIONS

To account for different populations of oscillators and their mutual interaction extensions of the KS model were proposed<sup>28,29</sup>. The intricate balance between the interactions of oscillators belonging to different populations gives rise to rich dynamical behaviour. In particular, these systems support chimera states in which one population is synchronised while the other is desynchronised<sup>34–38</sup>. Which of the two populations is synchronised and which is not depends on the initial condition. We consider here the dynamics of equally sized populations  $P_1$  and  $P_2$  of size  $N_1 = N_2 = N$ , and where each population is governed by the same dynamics in the sense that their native frequencies are drawn from the same distribution and their respective intra- and inter-population interactions are of equal strength. The dynamics of the phase oscillators is given by

$$\begin{aligned} \frac{d}{dt} \theta_i^{(1)} &= \omega_i^{(1)} + \frac{K}{N} \sum_{j \in P_1} \sin(\theta_j^{(1)} - \theta_i^{(1)} - \lambda) \\ &+ \frac{\kappa}{N} \sum_{j \in P_2} \sin(\theta_j^{(2)} - \theta_i^{(1)} - \lambda), \end{aligned} \quad (1)$$

$$\begin{aligned} \frac{d}{dt} \theta_j^{(2)} &= \omega_j^{(2)} + \frac{K}{N} \sum_{i \in P_2} \sin(\theta_i^{(2)} - \theta_j^{(2)} - \lambda) \\ &+ \frac{\kappa}{N} \sum_{i \in P_1} \sin(\theta_i^{(1)} - \theta_j^{(2)} - \lambda). \end{aligned} \quad (2)$$

Here  $\theta_i^{(\alpha)}$  denotes the phase of oscillator  $i = 1, \dots, N$  in population  $\alpha \in \{1, 2\}$ . The intrapopulation and inter-population coupling strengths are denoted by  $K$  and  $\kappa$ , respectively. We assume attractive forces and a stronger interaction between oscillators belonging to the same population with  $K > \kappa > 0$ . The parameter  $\lambda \in [0, \frac{\pi}{2}]$  accounts for a phase lag. Each oscillator is equipped with a native frequency drawn from a distribution  $g(\omega)$ . Note that through a change of coordinates into a rotating reference frame,  $\theta_i^{(\alpha)}(t) \rightarrow \theta_i^{(\alpha)}(t) - \bar{\omega}t$  with mean native frequency  $\bar{\omega} = \frac{1}{N} \sum \omega_i$ , we may assume without

loss of generality that the mean native frequency  $\bar{\omega}$  is zero. Here we consider normally distributed natural frequencies  $g(\omega) \sim \mathcal{N}(0, \sigma_\omega^2)$  for both populations, and in all computations we set  $\sigma_\omega^2 = 1$ . In the following we shall use greek sub- or superscripts to label populations and roman subscripts to label indices of oscillators.

The two-population KS model (1)–(2) undergoes a transition from desynchronised behaviour to synchronisation as the coupling strengths  $K$  and  $\kappa$  are gradually increased. At lower coupling strengths the oscillators exhibit desynchronised dynamics and a lack of coherent phase alignment. With increasing coupling strengths, the oscillators align their phases and oscillate with a common rotation frequency  $\Omega$ . Notably, this synchronisation typically involves both populations achieving coherent phase locking. However, depending on the particular choice of the intrapopulation coupling strength  $K$  and the interpopulation coupling strength  $\kappa$ , the system may exhibit symmetry breaking between the two populations and chimera states appear wherein one population achieves synchronisation while the other remains in a (relatively) desynchronised state<sup>35–38</sup>.

The collective behaviour of each of the populations is captured by complex mean-field variables  $z_\alpha$ , or equivalently by the real mean-field variables  $r_\alpha$  and  $\psi_\alpha$  for  $\alpha = 1, 2$ , with

$$z_\alpha := r_\alpha(t) e^{i\psi_\alpha(t)} = \frac{1}{N} \sum_{j \in P_\alpha}^N e^{i\theta_j^{(\alpha)}(t)}. \quad (3)$$

In particular, the order parameters  $\bar{r}_\alpha$  with

$$\bar{r}_\alpha = \lim_{T \rightarrow \infty} \frac{1}{T} \int_0^T r_\alpha(t) dt,$$

quantifies the degree of synchronisation within a population  $P_\alpha$ ; complete phase synchronisation with  $\theta_1^{(\alpha)} = \theta_2^{(\alpha)} = \dots = \theta_N^{(\alpha)}$  implies  $\bar{r}_\alpha = 1$ , whereas a fully desynchronised population with spread out phases implies  $\bar{r}_\alpha \sim \mathcal{O}(1/\sqrt{N})$ .

### A. Mean-field theory

Sakaguchi and Kuramoto<sup>10</sup> developed a mean-field theory for the case of a single population with uniform coupling for the order parameter  $r$  and the mean frequency  $\Omega$  of the synchronised cluster. Mean-field theory has been extended for the two population KS model (1)–(2)<sup>36,38,40,53</sup>. In the two-population KS model, we have mean-field variables for each population, i.e.  $z_\alpha$ , and the common mean frequency  $\Omega$ . The two-population KS model (1)–(2) can be written in terms of the complex mean field variables (3) as

$$\frac{d}{dt} \theta_i^{(1)} = \omega_i^{(1)} - \Omega + \text{Im} \left[ (Kz_1 + \kappa z_2) e^{-i\lambda} e^{-i\theta_i^{(1)}} \right] \quad (4)$$

$$\frac{d}{dt} \theta_i^{(2)} = \omega_i^{(2)} - \Omega + \text{Im} \left[ (Kz_2 + \kappa z_1) e^{-i\lambda} e^{-i\theta_i^{(2)}} \right], \quad (5)$$

where we moved into the frame of reference rotating with constant mean frequency  $\Omega$ . Each oscillator  $\theta_i^{(\alpha)}$  only couples to the other oscillators through the mean-field variables  $z_\alpha$  and  $\Omega$ .

In view of describing chimera states in which one of the two populations is synchronised whereas the other one is not, we shall without loss of generality assume that population  $P_1$  is (partially) synchronised and  $P_2$  is desynchronised, and we move into the frame of reference of the synchronised cluster with mean phase  $\psi_1$  and mean frequency  $\Omega$ . This implies  $z_1 e^{-i\psi_1} = r_1$  and motivates to introduce the phase-shifted order parameter of the desynchronised population

$$Z := z_2 = r_2 e^{i\Delta\psi}, \quad (6)$$

with  $\Delta\psi = \psi_2 - \psi_1$ .

The dynamics of the phases in (4)–(5) can now be expressed in terms of  $Z$ ,  $r_1$  and  $\Omega$  as

$$\frac{d}{dt} \theta_j^{(\alpha)} = \omega_j^{(\alpha)} - \Omega + \text{Im}(v_\alpha e^{-i\theta_j}) \quad (7)$$

for  $\alpha = 1, 2$ , where, for clarity of exposition, we introduce

$$\begin{aligned} v_1 &= (Kr_1 + \kappa Z)e^{-i\lambda}, \\ v_2 &= (KZ + \kappa r_1)e^{-i\lambda}. \end{aligned} \quad (8)$$

In the thermodynamic limit  $\Omega$ ,  $r_1$  and  $Z$  are constant. For constant mean-field parameters stationary solutions of (7)–(8) exist, provided the coupling strengths are sufficiently large ensuring

$$|\omega_j^{(\alpha)} - \Omega| < |v_\alpha|, \quad (9)$$

and are given by

$$\theta_j^{(\alpha)} = \arcsin\left(\frac{\omega_j^{(\alpha)} - \Omega}{|v_\alpha|}\right) + \arg(v_\alpha). \quad (10)$$

If, on the other hand, (9) is not satisfied, there are no stationary solutions, and instead the phases evolve according to (7)–(8).

In the thermodynamic limit  $N \rightarrow \infty$ , the phases for each population can be described by a probability density function  $\rho^{(\alpha)}(\theta, t; \omega)$  for  $\alpha = 1, 2$ , satisfying the continuity equation

$$\frac{\partial \rho^{(\alpha)}}{\partial t} + \frac{\partial}{\partial \theta} (\nu^{(\alpha)} \rho^{(\alpha)}) = 0, \quad (11)$$

where the vectorfields  $\nu^{(\alpha)}$  are given by the right-hand-side of (7) with

$$\nu^{(\alpha)} = \omega^{(\alpha)} - \Omega + \text{Im}(v_\alpha e^{-i\theta^{(\alpha)}}), \quad (12)$$

Stationary solutions satisfying  $\partial_t \rho^{(\alpha)} = 0$  depend on the equation parameters. Entrained oscillators with frequencies satisfying (9) are distributed according to the stationary density

$$\rho^{(\alpha)}(\theta; \omega) = \delta\left(\theta - \arcsin\left(\frac{\omega - \Omega}{|v_\alpha|}\right) - \arg(v_\alpha)\right), \quad (13)$$

whereas non-entrained oscillators with frequencies not satisfying (9) are distributed according to the stationary density

$$\rho^{(\alpha)}(\theta; \omega) = C^{(\alpha)} \frac{1}{\nu^{(\alpha)}}, \quad (14)$$

with normalisation constant  $C^{(\alpha)}$ , such that the density is high in regions where the phases spend much of their time (cf.(7)–(8)).

The order parameters  $r_1$  and  $Z = r_2 e^{i\Delta\psi}$  are given in the thermodynamic limit as

$$r_1 = \int_{-\infty}^{\infty} \int_0^{2\pi} e^{i\theta} \rho^{(1)}(\theta, t) g(\omega) d\theta d\omega \quad (15)$$

$$Z = \int_{-\infty}^{\infty} \int_0^{2\pi} e^{i\theta} \rho^{(2)}(\theta, t) g(\omega) d\theta d\omega. \quad (16)$$

The integration over the frequencies has to be split into the entrained and non-entrained ranges (9), each with their respective stationary density (13) or (14). After some algebraic manipulation, we obtain

$$\begin{aligned} r_1 &= i \int_{-\infty}^{\infty} \frac{v_1}{|v_1|} \left[ \frac{\omega - \Omega}{|v_1|} \right. \\ &\quad \left. - \sqrt{\frac{\omega - \Omega}{|v_1|} + 1} \sqrt{\frac{\omega - \Omega}{|v_1|} - 1} \right] g(\omega) d\omega \end{aligned} \quad (17)$$

$$\begin{aligned} Z &= i \int_{-\infty}^{\infty} \frac{v_2}{|v_2|} \left[ \frac{\omega - \Omega}{|v_2|} \right. \\ &\quad \left. - \sqrt{\frac{\omega - \Omega}{|v_2|} + 1} \sqrt{\frac{\omega - \Omega}{|v_2|} - 1} \right] g(\omega) d\omega, \end{aligned} \quad (18)$$

where we employ the convention that square roots of a negative real number have a positive imaginary part<sup>36,38,40,53</sup>. The complex equations (17)–(18) constitute self-consistency relations which allow to determine  $r_1$ ,  $Z$  and  $\Omega$ , at least numerically.

### III. NUMERICAL RESULTS FOR THE TWO-POPULATION KURAMOTO-SAKAGUCHI MODEL

To numerically integrate the two-population KS model (1)–(2) we prepare the initial conditions such that population  $P_1$  is synchronised with initial phase  $\theta_1^{(1)} = \theta_2^{(1)} = \dots = \theta_N^{(1)} = \psi_1 = 0$  and population  $P_2$  is desynchronised with initial phases uniformly sampled from  $[-\pi, \pi]$ . We employ the MATLAB `ode45` Runge-Kutta method to integrate (1)–(2) with relative and absolute tolerances set to  $2.2 \cdot 10^{-8}$ . To prevent an eventual formation of small clusters due to finite-size sample errors in the native frequencies<sup>54,55</sup>, we draw the two sets of  $N$  native frequencies  $\omega^{(\alpha)}$  equiprobably. We show results for chimera states with  $K = 100$ ,  $\kappa = 60$  and  $\lambda = \pi/2 - 0.075$ . For these parameters the evolution equations (7)–(8) support

a stable synchronised solution with constant mean-field variables.

To illustrate switching chimeras and how their existence depends on the number of oscillators  $N$ , we show in Figure 1 the temporal evolution of the order parameters  $r_1$  and  $r_2$  for  $N$  ranging from  $N = 6$  to  $N = 128$ . Switching between synchronised and desynchronised states is clearly seen. Switching events are not cyclic but appear randomly and the time between switches increases with  $N$ . We checked that for  $N = 21$  no chimera switching occurred for our initial condition when integrating for  $10^6$  time units. This suggests that chimera switching is induced by finite-size effects. It is further seen that the synchronised population exhibits less variation in the order parameter for larger numbers of oscillators. Figure 2 shows the mean switching time  $\bar{\tau}$ , estimated from 1,000 switching events, as a function of the system size  $N$ . The mean switching time  $\bar{\tau}$  increases exponentially with the network size  $N$ . A best-fit line suggests  $\bar{\tau} \sim \exp(0.889N)$ . This implies that for all practical purposes chimera switching is a finite-size effect. In Figure 3 we show the empirical probability  $P(\tau \geq \tau^*)$  of switching times  $\tau$  which are greater than or equal to some  $\tau^*$  for fixed  $N = 12$ , revealing an exponential distribution  $P(\tau \geq \tau^*) \approx \exp(-\frac{1}{\bar{\tau}}\tau^*)$  with  $\bar{\tau} \approx 486.8$ . This suggests that switching events occur independently and follow a Poisson process. We shall see that switching as well as the variance of the order parameter of the synchronised population is caused by an effective stochastic driving of the synchronised population by the desynchronised population.

To investigate how such an effective stochastic dynamics is generated in the deterministic two-population KS model, we examine the statistical behaviour of  $Z$ , which captures the driving interaction term of the synchronised population  $P_1$  with the desynchronised population  $P_2$  (cf. (7)). Figure 4 shows the empirical distribution of the driving term  $Z$  for a fixed number of oscillators  $N = 16$ . To generate the empirical distribution we simulated (1)–(2) for 10,000 time units, and determined  $Z$  from the desynchronised population, employing the symmetry of the model, irrespective if that is population  $P_1$  or  $P_2$ . The real and imaginary parts of  $Z$  are well approximated by a Gaussian with an empirical mean of  $\langle Z \rangle = 0.6243 + 0.1007i$ . The angular brackets  $\langle \cdot \rangle$  denote a temporal average.

Figure 5 shows how the variance of the real and imaginary components of  $Z$  varies with system size  $N$ . It is clearly seen that the variance decreases as  $1/N$ . The Gaussianity of the distribution and the scaling of the variance with approximately  $1/N$  suggests that finite-size fluctuations of  $Z$  around its thermodynamic mean  $\langle Z \rangle$  are governed by an underlying central limit theorem and

$$\zeta = \sqrt{N}(Z - \langle Z \rangle) + o(1/\sqrt{N}) \quad (19)$$

is effectively a stochastic complex-valued Gaussian process. Hence, to obtain an effective stochastic dynamics

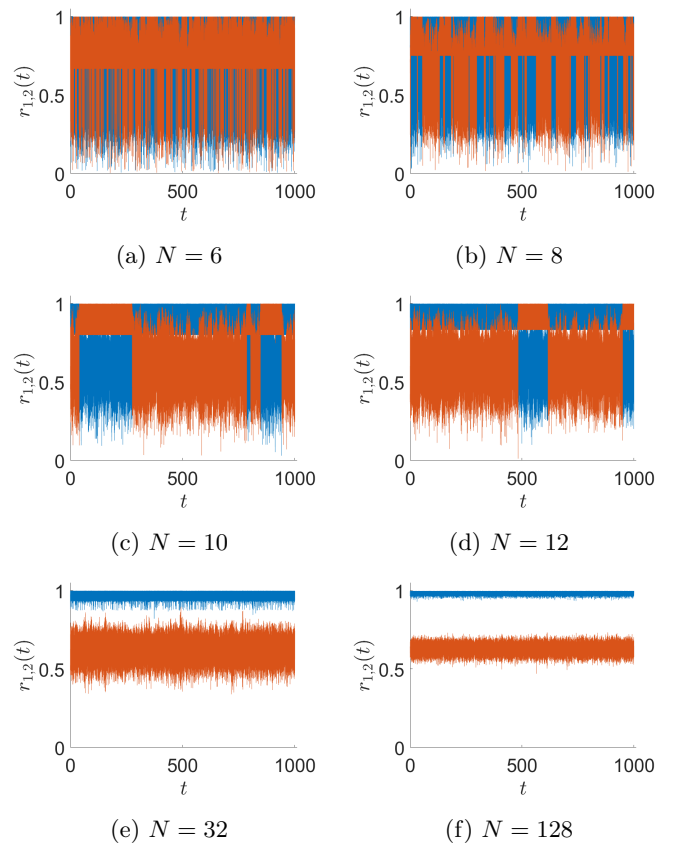


FIG. 1: Order parameters  $r_1$  (blue) and  $r_2$  (orange) for the two-population KS model (1)–(2) exhibiting switching chimeras as a function of time for various numbers of oscillators  $N$ . Equation parameters are  $K = 100$ ,  $\kappa = 60$  and  $\lambda = \frac{\pi}{2} - 0.075$  and native frequencies  $\omega$  are drawn equiprobably from a standard normal distribution  $\mathcal{N}(0, 1)$ .

capable of inducing the observed chimera switching and the approximation of  $Z(t)$  by a Gaussian process, we require the number of oscillators to be sufficiently large for the central limit theorem to hold and sufficiently small so that the variance of the effective noise is nonnegligible. In Figure 6, we show how the empirical histograms of  $\zeta$ , obtained by simulations of (1)–(2) over 4,000 time units, converge for increasing system size  $N$ . It is clearly seen that the fluctuations are not Gaussian for  $N = 8$ , which is too small for the central limit theorem to work. For system sizes larger than  $N = 12$ , the distribution of the components of  $\zeta$  becomes approximately Gaussian, and indeed becomes more Gaussian as  $N$  increases. It is seen that increasing the system size leads to a decrease in the variance of the Gaussian, with saturation occurring around  $N = 48$ . For such systems with  $N = 48$ , however, the phenomenon of switching is non-existent for all practical purposes. We hence limit the numerical study of switching to systems of  $N \leq 16$ .

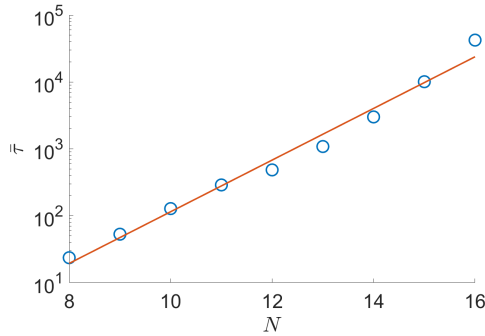


FIG. 2: Mean switching time  $\bar{\tau}$  as a function of the number of oscillators  $N$  (blue circles). The orange line shows a best-fit exponential regression model with  $\bar{\tau} = \exp(0.889N - 4.15)$ . Equation parameters are as in Figure 1.

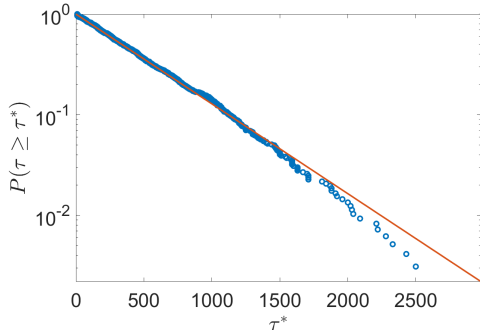


FIG. 3: Probability of switching times  $P(\tau \geq \tau^*)$  as a function of  $\tau^*$  for a network of size  $N = 12$ , estimated from 968 switching events. Blue circles denote samples of the switching times. The orange line shows a best-fit regression model corresponding to  $P(\tau \geq \tau^*) = \exp(-\tau^*/\bar{\tau})$  with  $\bar{\tau} \approx 486.8$ . Equation parameters are as in Figure 1.

Recall that  $Z$  encodes the effect of the desynchronised population onto the phases of the synchronised population, i.e. the second sum in the right-hand side of (1) using our convention that population  $P_1$  is the synchronised one. This opens up the way to employ the stochastic model reduction framework developed in<sup>51</sup> to model the dynamics of the phases of the synchronised population. This will be achieved in Section V. To allow for an analytical approximation of the mean switching time we will need to determine the critical size of fluctuations that are sufficient to induce the synchronised population to switch. The asymptotic state of population  $P_1$  sensitively depends on the initial condition of the desynchronised population  $P_2$ . Figure 7 shows the dependency of the average value of  $\Delta r := r_2 - r_1 = |Z| - r_1$  on the initial value  $Z_0 = Z(0)$  for a network with  $N = 512$  oscillators. Results were obtained by simulating the

two-population KS model (1)–(2) for 10 time units, for which the order parameters have equilibrated. We chose non-equilibrium initial conditions for population  $P_1$  with  $\theta_1^{(1)} = \theta_2^{(1)} = \dots = \theta_N^{(1)}$ , and random initial conditions for population  $P_2$  with  $\theta_j^{(2)}$ ,  $j = 1, \dots, N$ , drawn from the stationary density (14) consistent with a specified value of  $Z_0$ . We observe two scenarios: either  $P_1$  is synchronised and  $P_2$  is desynchronised (blue region), or  $P_1$  is desynchronised and  $P_2$  is synchronised (yellow region). The boundary separating these two states and its distance to the fixed point  $\langle Z \rangle$  (red cross in Figure 7) determines the size of critical fluctuations of  $Z$ . The near circular boundary suggests that the critical fluctuation size is approximated by the average radius of the basin boundary which is estimated as  $q^* = 0.386$ . In the following Section we employ mean-field theory to determine an analytical expression for the critical size  $q^*$ .

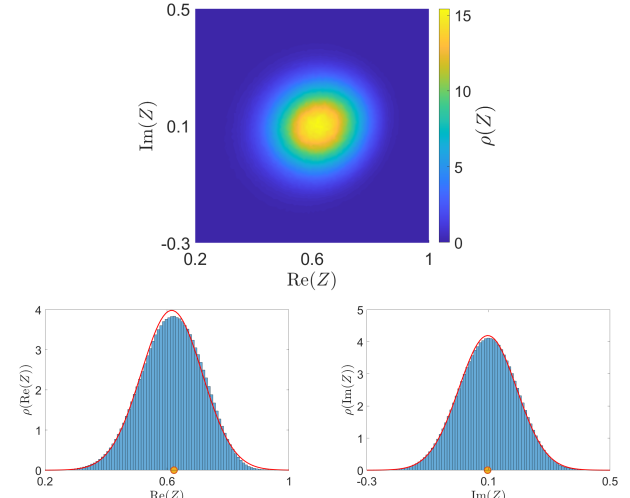


FIG. 4: Empirical joint (top) and marginal (bottom) distributions of  $Z$  obtained from simulating (1)–(2) with  $N = 16$ . The filled orange circles denote the thermodynamic value of the real and imaginary part of  $Z$  as calculated from the self-consistency relations (17)–(18) of the mean-field theory. The red lines are best-fit Gaussian distributions. Equation parameters are as in Figure 1.

#### IV. DETERMINISTIC MODEL REDUCTION

Using the celebrated Ott-Antonsen ansatz valid in the thermodynamic limit, the two-population KS model (2)–(2) was shown to support stable chimeras, breathing chimeras, and saddle-node and Hopf bifurcations of chimera states<sup>36–38,40,53</sup>. We will follow Laing<sup>37</sup> and derive here a low-dimensional dynamical model for the complex order parameters (3) in a perturbative approach. Using (7)–(8) we obtain the evolution equation for the

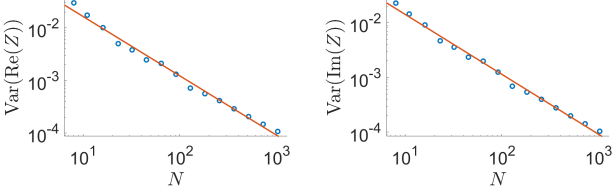


FIG. 5: Variance of the real (left) and imaginary (right) component of  $Z$  as a function of the number of oscillators  $N$ . The orange lines show a power law best fit indicating a scaling with  $N^{-1.13}$  and  $N^{-1.10}$  for the real and imaginary parts, respectively. Equation parameters are as in Figure 1.

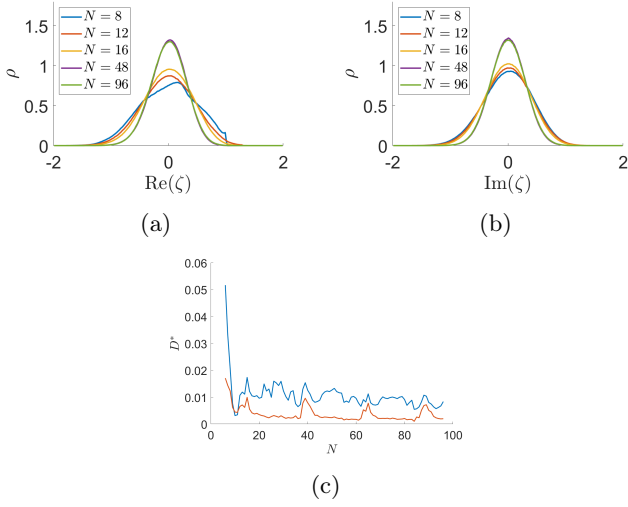


FIG. 6: Empirical distributions of the real (a) and imaginary (b) part of  $\zeta$  obtained from simulating (1)–(2) for  $N = 8$ ,  $N = 12$ ,  $N = 16$ ,  $N = 48$  and  $N = 96$ , showing convergence with increasing system size  $N$ . The corresponding Kolmogorov–Smirnov statistics for the distributions of the real (blue) and imaginary (orange) components of  $\zeta$  quantifies the convergence to a Gaussian with increasing  $N$  (c).

Equation parameters are as in Figure 1.

order parameters

$$\frac{d}{dt}z_\alpha = iz_\alpha^{(1,1)} + \frac{1}{2}(v_\alpha - v_\alpha^*z_\alpha^{(2,0)}), \quad (20)$$

for the two populations with  $\alpha = 1, 2$ , where we write (8) as

$$\begin{aligned} v_1 &= (Kz_1 + \kappa z_2)e^{-i\lambda}, \\ v_2 &= (Kz_2 + \kappa z_1)e^{-i\lambda}, \end{aligned} \quad (21)$$

and  $z_\alpha^{(m,n)}$  is defined as

$$z_\alpha^{(m,n)} = \frac{1}{N} \sum_{j=1}^N (\omega_j^{(\alpha)})^n \exp(im\theta_j^{(\alpha)}), \quad (22)$$

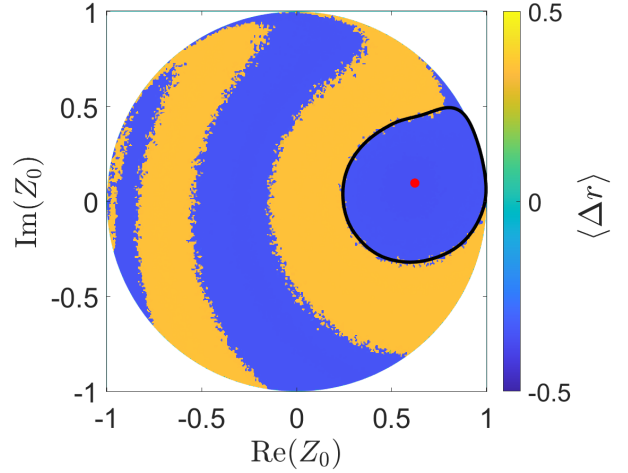


FIG. 7: Time-averaged difference of the order parameters,  $\langle \Delta r \rangle := \langle r_2 - r_1 \rangle = \langle |Z| - r_1 \rangle$ , as a function of the initial condition  $Z_0 = Z(0)$  of the two-population KS model (1)–(2). The  $N = 512$  oscillators were initialised with  $\theta_j^{(1)}(0) = 0$  for all  $j \in P_1$  and  $\theta_j^{(2)}(0)$  were drawn from the stationary distribution for non-entrained oscillators (14). The temporal mean is estimated during the time window  $t \in [2.5, 10]$ . The thermodynamic equilibrium with  $\langle Z \rangle = 0.6230 + 0.0972i$  is shown as a red dot. The blue region denotes initial conditions which evolve into a state where  $P_1$  is synchronised and  $P_2$  is desynchronised, and the yellow region denotes initial conditions which evolve into states where  $P_1$  is desynchronised and  $P_2$  is synchronised. The black curve approximates the boundary separating these two states where we employed a Gaussian kernel to smooth the curve. The boundary has an average radius of  $q^* = 0.386$ . Equation parameters are as in Figure 1.

for  $m, n \in \mathbb{N}$ . Note that  $z_\alpha^{(1,0)} = z_\alpha$ .

Equation (20) is not a closed equation for the complex order parameters  $z_\alpha$  but instead presents a closure problem whereby higher and higher orders of the order parameter are required to close the equation with

$$\frac{d}{dt}z_\alpha^{(m,n)} = m(iz_\alpha^{(m,n+1)} + \frac{1}{2}(v_\alpha z_\alpha^{(m-1,n)} - v_\alpha^* z_\alpha^{(m+1,n)})). \quad (23)$$

We assume again without loss of generality that population  $P_1$  is synchronised with  $z_1 = r_1 e^{i\psi_1}$  and population  $P_2$  is desynchronised with  $z_2 = r_2 e^{i\psi_2}$ . In order to close the equations for  $z_{1,2}$  we truncate the system by employing the following two approximations

$$z_\alpha^{(2,0)} = z_\alpha^2, \quad z_\alpha^{(1,1)} = 0, \quad (24)$$

for  $\alpha = 1, 2$ . We checked the validity of these approximations numerically (not shown), and provide a heuristic formal justification in Appendix A. Substituting

the approximations (24) into (20) we obtain the closed Ott-Antonsen equations<sup>18,38,40,53</sup> for the dynamics of the complex order parameters with

$$\frac{d}{dt}z_\alpha = \frac{1}{2}(v_\alpha - v_\alpha^* z_\alpha^2) \quad (25)$$

for  $\alpha = 1, 2$ . The closed equations (25) exhibit a Hopf bifurcation upon varying the intrapopulation coupling strength  $K$ <sup>36</sup>. Figure 8 shows the temporal evolution of the order parameters  $r_{1,2} = |z_{1,2}|$  under the Ott-Antonsen dynamics (25). The dynamics exhibits chimera states in the reduced model characterised by a synchronised population  $P_1$  with  $r_1 = 1$  and a desynchronised population  $P_2$ . The desynchronised population either has a stationary limiting state (with respect to the reference frame  $\Omega$ ) with  $r_2 \approx 0.62$  or supports a stable limit cycle oscillating around a similar value. Such breathing chimera states are supported as well in the full two-population KS model (1)–(2). Our focus here is the case of a stationary fixed point. The stationary fixed point of the reduced Ott-Antonsen equation (25) is  $Z = 0.6096 + 0.0934i$ , matching well the results of the full model (1)–(2) with  $\langle Z \rangle = 0.6243 + 0.1007i$  (cf. Figure 4).

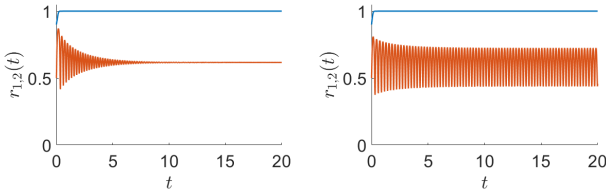


FIG. 8: Order parameters  $r_1$  (blue) and  $r_2$  (orange) as a function of time for the reduced deterministic mean-field dynamics (25) with  $K = 100$ ,  $\kappa = 60$  and  $\lambda = \pi/2 - 0.075$  (left) and  $K = 90$ ,  $\kappa = 50$  and  $\lambda = \pi/2 - 0.1$  (right). We used  $z_1(0) = 0.9$  and  $z_2(0) = 0.5$  to generate the chimera state in the reduced model.

The rapid relaxation of  $r_1$  to its stable equilibrium at  $r_1 = 1$  suggests to make the additional simplifying assumption of  $r_1 = 1$ , which allows us to express  $Z$  as  $Z = z_2/z_1 = r_2 e^{i\psi_1}$  (with  $\Delta\psi = \psi_1 - \psi_2$ ), which evolves according to

$$\begin{aligned} \frac{d}{dt}Z &= \frac{(KZ + \kappa)e^{-i\lambda} - (KZ|Z|^2 + \kappa Z^2)e^{i\lambda}}{2} \\ &\quad - \frac{(KZ + \kappa Z^2)e^{-i\lambda} - (KZ + \kappa|Z|^2)e^{i\lambda}}{2} \\ &= \kappa \cos \lambda \times \\ &\quad \left(1 - Z^2 - \frac{1 + i \tan \lambda}{2}(1 - \frac{K}{\kappa}Z)(1 - |Z|^2)\right). \quad (26) \end{aligned}$$

The real scalar factor  $\kappa \cos \lambda$  controls the time scale. Figure 9 shows the basin of attraction for the stationary

desynchronised stationary fixed point and the desynchronised limit cycle from Figure 8 obtained from the reduced mean-field dynamics (26). This compares well with the corresponding plots for the full two-population KS model (1)–(2) (cf. Figure 7).

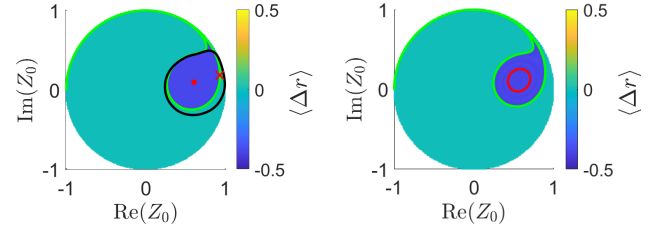


FIG. 9: Asymptotic value of the difference of the time-averaged order parameters,

$\Delta r := r_2 - r_1 = |Z| - r_1$ , as a function of the initial condition  $Z_0$  for the reduced deterministic mean-field model (26). Left: Initial conditions in the blue region evolve to a fixed point with  $\hat{Z} = 0.6096 + 0.0934i$  (red dot) for  $K = 100$ ,  $\kappa = 60$  and  $\lambda = \pi/2 - 0.075$ . Initial conditions in the bluegreen region evolve into a fully synchronised state with  $Z = 1$ . The boundary between the blue and green region is marked in light green. The red cross on the boundary marks a second unstable fixed point. We have overlaid the corresponding boundary curve (black) obtained from the full two-population KS model (1)–(2) for comparison (cf. Figure 7). Right: Initial conditions in the blue region evolve to a limit cycle (red loop) for  $K = 90$ ,  $\kappa = 50$  and  $\lambda = \pi/2 - 0.1$ . Initial conditions in the bluegreen region evolve into a fully synchronised state with  $Z = 1$ . Equation parameters are as in Figure 8.

To approximate the critical size of fluctuations of  $Z(t)$ ,  $q^*$ , that may lead to switching, we derive an approximation for the temporal evolution of the radial component  $q := |Z - \hat{Z}|$ , where  $\hat{Z}$  is the stable fixed point of (26). Averaging over the angular component, we obtain

$$\begin{aligned} \frac{d}{dt}q &\approx Q(q) \\ &:= \frac{\left(\int_0^{2\pi} \frac{\text{Re}(F(\hat{Z} + q e^{i\vartheta}) e^{-i\vartheta})}{\text{Im}(F(\hat{Z} + q e^{i\vartheta}) e^{-i\vartheta})} d\vartheta\right)}{\left(\int_0^{2\pi} \frac{1}{\text{Im}(F(\hat{Z} + q e^{i\vartheta}) e^{-i\vartheta})} d\vartheta\right)}, \quad (27) \end{aligned}$$

where  $F(Z) := \frac{d}{dt}Z$  is given by the right-hand side of (26). Figure 10 shows that  $Q(q)$  is well approximated by a cubic function for  $q \lesssim q^*$  with  $q^* \approx 0.339$ . At  $q^*$  there is a second fixed point  $Z^*$  of (26) with  $F(Z^*) \equiv 0$  leading to a divergence of  $Q(q)$ . This second fixed point  $Z^*$  is unstable and is located on the boundary of the basin of attraction of the fixed point (red cross on the green line in Figure 9). This suggests that  $q^* = |Z^* - \langle Z \rangle| = 0.339$ .

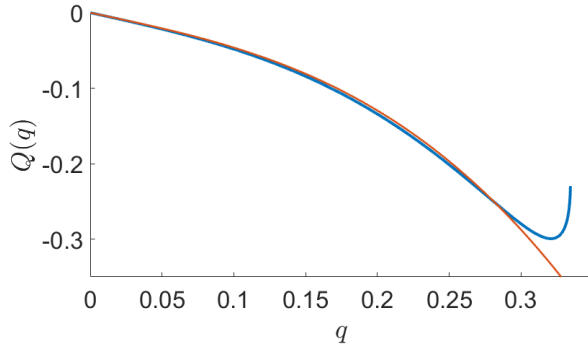


FIG. 10: Approximate temporal derivative of  $q = |Z - \hat{Z}|$ ,  $Q(q)$ , as a function of  $q$  obtained from numerically solving (27) for  $K = 100$ ,  $\kappa = 60$ ,  $\lambda = \frac{\pi}{2} - 0.075$  (blue curve). A best-fit cubic approximation is shown as a red curve.

## V. STOCHASTIC MODEL REDUCTION

We follow here the framework of Yue and Gottwald<sup>51</sup> and formulate a closed stochastic equation for the synchronised population, which we assume without loss of generality to be population  $P_1$ . Dropping superscripts, we write the dynamics of the two-population KS model (4) for population  $P_1$  as

$$\frac{d}{dt}\theta_i = \omega_i - \Omega + \text{Im} \left[ (K r_1 + \kappa Z) e^{-i(\theta_i + \lambda - \psi_1)} \right]. \quad (28)$$

The numerical results in Section III and (19) suggest to model  $Z$  by a Gaussian process  $\zeta_t$  as in (19). We approximate  $\zeta_t$  by an Ornstein-Uhlenbeck (OU) process  $\hat{\zeta}(t)$ , the parameters of which are chosen to match the mean and the covariance function of the true  $Z$ . We hence replace the deterministic evolution equation (28) by the stochastic evolution equation

$$\begin{aligned} \frac{d}{dt}\theta_i &= \omega_i - \Omega \\ &+ \text{Im} \left[ \left( K r_1 + \kappa \left( \langle Z \rangle + \frac{1}{\sqrt{N}} \hat{\zeta} \right) \right) e^{-i(\theta_i + \lambda - \psi_1)} \right], \end{aligned} \quad (29)$$

with a complex Gaussian mean-zero OU process

$$d\hat{\zeta} = -\gamma \hat{\zeta} dt + \sigma dW(t) \quad (30)$$

with complex drift and diffusion coefficients  $\gamma$  and  $\sigma$ , respectively, and a complex Wiener process  $W(t)$ . The mean-value  $\langle Z \rangle$  can be either numerically estimated from long-time simulations or approximated by the results from the mean-field theory in Section II A. For the parameters we consider here with  $N = 12$ ,  $K = 100$ ,  $\kappa = 60$  and  $\lambda = \pi/2 - 0.075$  and a standard Gaussian native frequency distribution with mean zero and variance  $\sigma_\omega^2 = 1$  we obtain  $\langle Z \rangle = 0.6227 + 0.1000i$

from a long-time simulation of the full two-population KS model (4)-(5) over 10,000 time units which is nicely reproduced by the reduced deterministic system (25) with  $\langle Z \rangle = 0.6096 + 0.0934i$ . In the following simulations we employ the thermodynamic limit.

### A. Approximation of fluctuations $\zeta$ by an Ornstein-Uhlenbeck process $\hat{\zeta}$

Any Gaussian process is entirely determined by its mean and its covariance function. It is convenient to consider a 2-dimensional Wiener process and treat  $\zeta$  as a 2-dimensional column vector with real entries. The complex drift and diffusion coefficients are then represented by  $2 \times 2$  matrices  $\Gamma$  and  $\Sigma$ , respectively. To avoid notational confusion we denote this real-valued stochastic process of fluctuations as  $\vec{\zeta}$ . The covariance function of the full two-population KS model (1)–(2) is defined as

$$\begin{aligned} R(t) &= \text{cov}(\vec{\zeta}(s+t), \vec{\zeta}(s)) \\ &= \langle \vec{\zeta}(s+t) \vec{\zeta}(s)^\top \rangle_s \end{aligned} \quad (31)$$

and is a real-valued  $2 \times 2$  matrix. The covariance matrix  $R(t)$  can be determined numerically from a long-time simulation. The covariance function of an approximating OU process (30) is given explicitly as

$$R_{\text{OU}}(t) = \exp(-\Gamma t) \langle \vec{\zeta}_0 \vec{\zeta}_0^\top \rangle_{\text{OU}}, \quad (32)$$

where  $\vec{\zeta}_0$  are random variables drawn from the density of the 2-dimensional OU-process (30) and the angular brackets  $\langle \cdot \rangle_{\text{OU}}$  denote the average with respect to the stationary Gaussian density of the OU-process. For simplicity, we impose a symmetry assumption between the real and imaginary parts of the drift and diffusion matrices and set

$$\Gamma = \text{Re}(\gamma) \mathbf{I} + \text{Im}(\gamma) \mathbf{J} \quad (33)$$

$$\Sigma = \sigma \mathbf{I} \quad (34)$$

with identity matrix  $\mathbf{I}$  and skew-symmetric matrix  $\mathbf{J}$  with  $J_{12} = -J_{21} = 1$  and  $J_{11} = J_{22} = 0$ , rather than considering more general drift and diffusion matrices as done in<sup>51</sup>. The averages in the covariance function of the OU process (32) can be calculated explicitly, see for example<sup>51</sup>. The aim is to determine the parameters of the OU-process (30), i.e. the coefficients  $\gamma$  and  $\sigma$ , such that the covariance function of the OU process (32) best approximates the actual covariance function (31). The covariance function  $R(t)$  of the fluctuations of the full two-population KS model exhibits small-scale variations that quickly decay as shown in Figure 11. This suggest to only fit the covariance functions for times larger than  $t = t_{\min}$  after which the fast-scale processes have decayed. To find the approximating OU-process we therefore minimise the ob-

jective function

$$E(\gamma, \sigma) = \sum_{i,j}^2 \int_{t_{\min}}^{t_{\max}} \|R_{i,j}(t) - R_{\text{OU},i,j}(t)\|^2 dt. \quad (35)$$

We use the MATLAB function `fminsearch` to perform the nonlinear least-square optimisation problem for (35). We use  $t_{\min} = 0.5$  and  $t_{\max} = 1$ . We initialise  $\gamma = \gamma_0$  as the eigenvalue of the linearisation of the deterministic approximate mean-field dynamics (26) around the stationary solution, which we numerically estimated as  $\gamma_0 = 0.42 - 28.98i$ . We found that the optimisation was less sensitive to the choice of the initial diffusion coefficient  $\sigma$ ; we chose  $\sigma$  such that  $\sigma^2/(2N \text{Re}(\gamma)) = 0.005$ . The numerical minimisation of (35) yields

$$\gamma = 1.75 - 25.34i \quad \text{and} \quad \sigma = 0.574. \quad (36)$$

Figure 11 shows how the fitted covariance function  $R_{\text{OU}}(t)$  well approximates the actual covariance function  $R(t)$  for  $t > t_{\min} = 0.5$ . This justifies our approximation of the fluctuations  $\zeta$  by a Gaussian OU process.

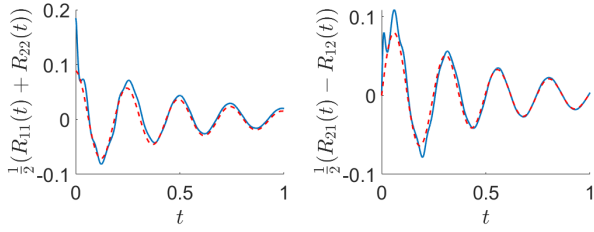


FIG. 11: Covariance functions  $R(t)$  for the (two-dimensional) fluctuations  $\zeta$  of the full two-population KS model (1)–(2) (blue) and  $R_{\text{OU}}(t)$  for the OU-approximation  $\hat{\zeta}$  with the best-fit parameters (36) (dashed red). Equation parameters are  $N = 12$ ,  $K = 100$ ,  $\kappa = 60$  and  $\lambda = \frac{\pi}{2} - 0.075$  and native frequencies  $\omega$  are drawn equiprobably from a standard normal distribution  $\mathcal{N}(0, 1)$ .

## B. A Kramers problem for the mean switching time

The reduced stochastic model (29)–(30) suggests that switching is induced by sufficiently large fluctuations  $\zeta$ . Figure 7 revealed that such fluctuations from the thermodynamic mean  $\langle Z \rangle$  (denoted by the red dot) are those that cross the basin boundary denoted by the black line. An approximation for this basin boundary is a circle with radius  $q^*$  which we estimated numerically from the full two-population KS model as  $q^* = 0.386$  and from our reduced deterministic mean-field model (26) and its averaged approximation (27) as  $q^* = 0.339$ . This suggests to compute the mean switching time by determining the average time it takes the OU process (30) to generate fluctuations of size  $q^*$  when started at equilibrium with

$q = 0$ . This is the classic setting of a Kramers problem<sup>52</sup> for a stochastic differential equation for the azimuthally averaged fluctuation

$$q = \frac{1}{\sqrt{N}} |\zeta|. \quad (37)$$

Employing Itô's formula and the OU process (30), we find that fluctuations  $q$  evolve according to

$$\begin{aligned} dq &= \left( \frac{\sigma^2}{2qN} - \text{Re}(\gamma)q \right) dt + \frac{\sigma}{\sqrt{N}} dB_t \\ &= -\frac{d}{dq} V(q) + \frac{\sigma}{\sqrt{N}} dB_t \end{aligned} \quad (38)$$

with real-valued 1-dimensional Wiener process  $B_t$  and potential

$$V(q) = -\frac{\sigma^2}{2N} \log(q) + \frac{1}{2} \text{Re}(\gamma) q^2. \quad (39)$$

The mean switching time  $\bar{\tau}$  is expressed as

$$\bar{\tau} = 2\tau_e \quad (40)$$

where the exit time  $\tau_e$  is the mean time it takes for a trajectory  $q(t)$  with initial condition  $q(0) = 0$  to reach  $q(\tau_e) = q^*$ . The exit time  $\tau_e$  is the solution of Kramers problem for (38)

$$\mathcal{L}\tau_e = -1 \quad (41)$$

with the generator associated with the stochastic process (27)

$$\mathcal{L} = -\frac{d}{dq} V(q) \partial_q + \frac{\sigma^2}{2} \partial_{xx}, \quad (42)$$

and boundary conditions  $\partial\tau_e/\partial q(q = 0) = 0$  and  $\tau_e(q^*) = 0$ . The solution of the Kramers problem (41) is explicitly written as

$$\tau_e = \frac{1}{\text{Re}(\gamma)} \int_0^{q^*} \frac{1}{u} \left[ \exp\left(\frac{N \text{Re}(\gamma)}{\sigma^2} u^2\right) - 1 \right] du, \quad (43)$$

which can be evaluated numerically. Note that the exit time (and hence the mean switching time) is determined by the stochastic dynamics of the fluctuations (27). Information about the synchronised population only enters via the value of  $q^*$ .

In the next Section we show that the reduced stochastic model (29)–(30) is able to quantitatively capture the statistical behaviour of the deterministic two-population KS model (4)–(5), including the mean switching time.

## VI. COMPARISON OF THE REDUCED STOCHASTIC MODEL WITH THE FULL TWO-POPULATION KURAMOTO-SAKAGUCHI MODEL

We now assess the ability of the reduced stochastic model of the synchronised population (29)–(30) to describe the dynamics of the full two-population KS model

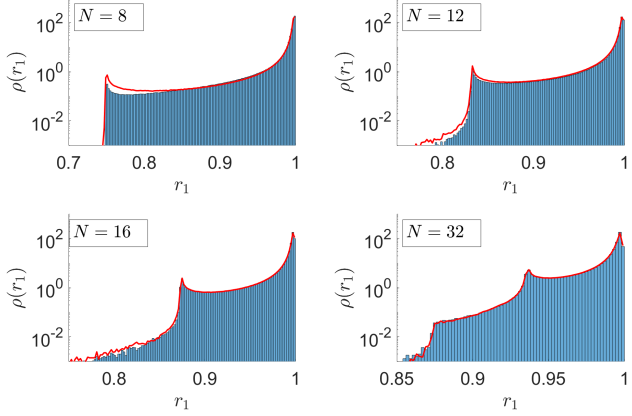


FIG. 12: Comparison of the empirical histograms for the order parameter  $r_1$  of the synchronised population obtained from a single trajectory of the full two-population KS model (1)–(2) (blue histogram) and from the reduced stochastic model (29)–(30) (red line) for  $N = 8, 12, 16$  and  $32$ . A log scale has been applied to the  $y$ -axis. Equation parameters are as in Figure 1.

(1)–(2). We begin by first assessing how the model is able to describe the invariant density of the order parameter  $r_1$  and of the relative phases  $\theta_i - \psi_1$ . The reduced stochastic model (29)–(30) is integrated with a time step of  $\Delta t = 0.001$  using a 4th order Runge-Kutta scheme with pregenerated noise  $\hat{\zeta}$ . To generate the OU process  $\hat{\zeta}$  we employ a numerical scheme that exactly reproduces the transition probabilities independent of the employed time step (see Appendix B for details).

We first show in Figure 12 a comparison of the empirical histogram of the order parameter  $r_1$  for the synchronised population for  $N = 8, 12, 16$  and  $N = 32$ . Remarkably, even  $N = 8$  oscillators are sufficient to allow for the reduced stochastic model to reliably approximate the density of the order parameter.

The empirical histograms shown in Figure 12 have pronounced peaks. These peaks are caused by one or more oscillators of the synchronised population to desynchronise, which causes isolated drops of the order parameter as illustrated in Figure 13, which shows the order parameter  $r_1$  as a function of time, during periods over which no switching occurred. The amplitude of the peaks can be explicitly estimated via a simple argument: Under the assumption that a single oscillator, which we label here without loss of generality as  $\theta_N$ , desynchronises with  $\theta_N = \pi$  from the synchronised population, which we approximate by  $\theta_1 = \theta_2 = \dots = \theta_{N-1} = 0$ , the order parameter can be approximated as  $r_1 \approx 1 - \frac{2}{N}$ , which fits the observed peaks in the histograms depicted in Figure 12 very well, in particular for  $N > 12$ . The frequency of the dips and their size are well recovered by the reduced stochastic model for  $N \geq 12$ .

The reduced stochastic model (29)–(30) is further able to reproduce the statistics of the fluctuations of the syn-

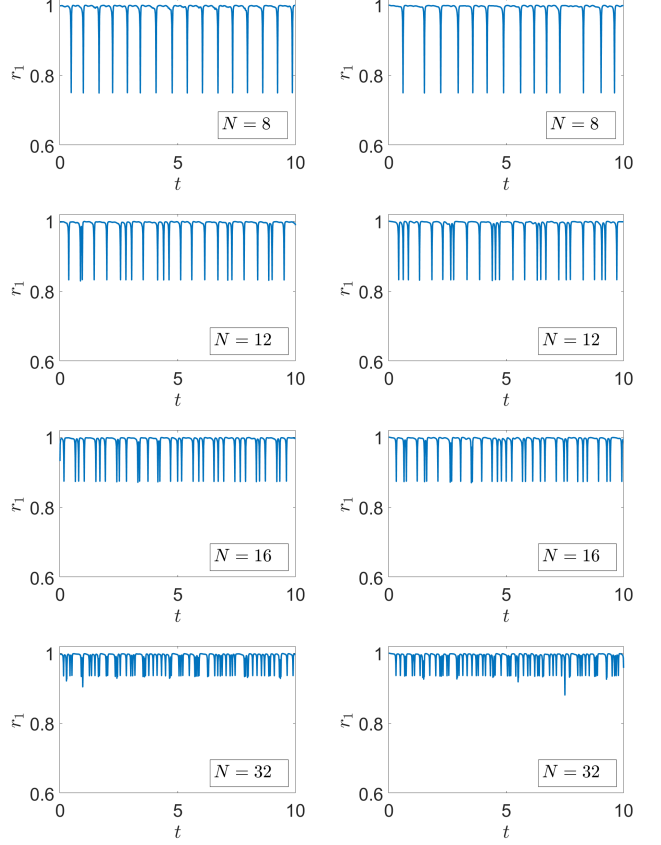


FIG. 13: Order parameter  $r_1(t)$  as a function of time of the full two-population KS model (1)–(2) (left column) and of the reduced stochastic model (29)–(30) (right column) for  $N = 8, 12, 16$  and  $32$ . Equation parameters are as in Figure 1.

chronised phases around their mean,  $\theta_i - \psi_1$ . Figure 14 shows the empirical histograms of  $\theta_i - \psi_1$  for  $N = 8, 12, 16$  and  $N = 32$ , over all oscillators of the synchronised population. It is seen again that even for the small system size with  $N = 8$  the reduced stochastic model is able to describe the statistical properties of the full two-population KS model (1)–(2). The accuracy of the reduced stochastic model increases, as expected, with increasing system size  $N$ . The histograms of the full two-population KS model exhibit isolated sharp peaks for  $N < 16$  at the mean of the phases of individual oscillators. These undulations get smeared out for a sufficiently large number of oscillators.

To see in how far the reduced stochastic model captures the statistics of individual oscillators we show in Figures 15 and 16 the mean and variance for each synchronised oscillator, and in Figure 17 the average effective frequency  $\bar{\nu}_i := \langle \theta_i(t) \rangle$  for each synchronised oscillator. Remarkably, the mean of the fluctuations is well approximated by the reduced stochastic model even for  $N = 8$ . These figures show that the synchronised population involves rogue oscillators at the edge of the population,

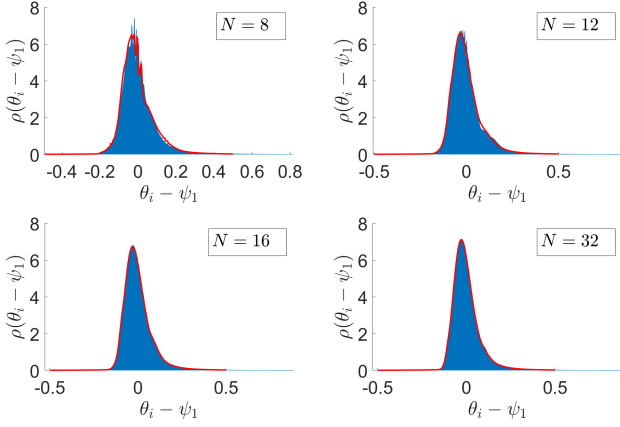


FIG. 14: Comparison of the empirical histograms for the fluctuations of the synchronised phases around their mean,  $\theta_i - \psi_1$ , obtained from a single trajectory of the full two-population KS model (1)–(2) (blue histogram) and of the reduced stochastic model (29)–(30) (red line) for  $N = 8, 12, 16$  and  $32$ . Equation parameters are as in Figure 1.

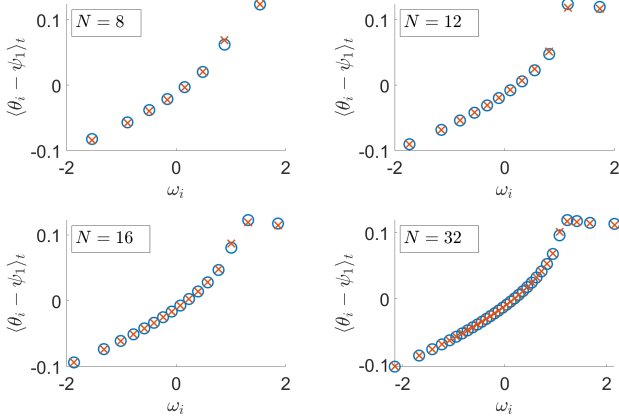


FIG. 15: Mean of the fluctuations of the synchronised phases around their mean,  $\theta_i - \psi_1$ , as a function of their native frequencies  $\omega_i$  for the full two-population KS model (1)–(2) (blue circles) and for the reduced stochastic model (29)–(30) (red crosses) for  $N = 8, 12, 16$  and  $32$ . Equation parameters are as in Figure 1.

which oscillate with markedly different mean rotation frequencies and mean phases. The reduced stochastic model is able to capture the mean phase as well as the variance of all oscillators, even of the rogue oscillators very well.

Figure 18 shows the mean switching time  $\bar{\tau}$  as a function of the system size  $N$ . We compare the mean switching time of the full two-population KS model (1)–(2) with the expected switching times  $\bar{\tau} = 2\tau_e$  of the reduced stochastic model (29)–(30) which we estimate from the solution of Kramers problem (43) for both  $q^* = 0.386$  as estimated from the full two-population KS model (1)–(2)

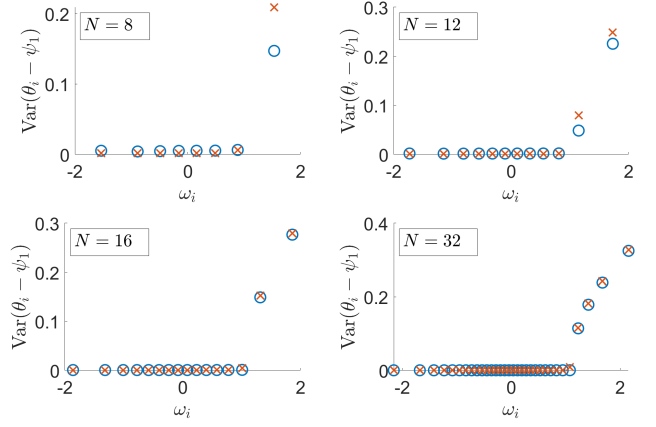


FIG. 16: Variance of the fluctuations of the synchronised phases around their mean,  $\theta_i - \psi_1$ , as a function of their native frequencies  $\omega_i$  for the full two-population KS model (1)–(2) (blue circles) and for the reduced stochastic model (29)–(30) (red crosses) for  $N = 8, 12, 16$  and  $32$ . Equation parameters are as in Figure 1.

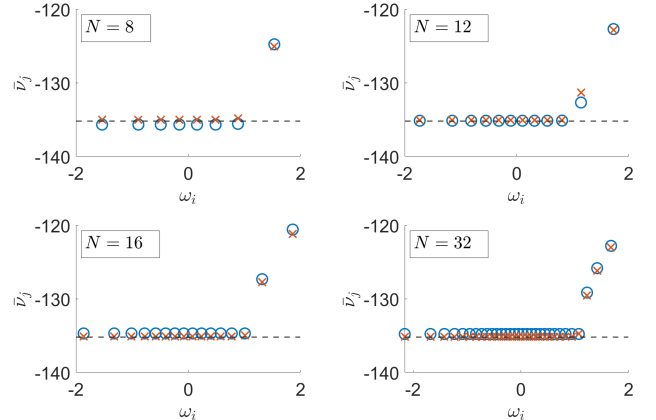


FIG. 17: Mean rotation frequency  $\bar{\nu}_i$  of the synchronised oscillators as a function of their native frequencies  $\omega_i$  for the full two-population KS model (1)–(2) (blue circles) and for the reduced stochastic model (28)–(29) (red crosses) for  $N = 8, 12, 16$  and  $32$ . The dashed lines denote the mean frequency  $\Omega$  as calculated from the self-consistency relations (17)–(18) of the mean-field theory. Equation parameters are as in Figure 1.

(cf. Figure 7) and for  $q^* = 0.339$  as estimated from the reduced deterministic mean-field model (cf. Figures 9 and 10). For each value of  $N$  the mean switching time is estimated over 1,000 switching events in the full model. It is remarkable how the simple approximation captures the mean switching time reasonably well. Setting a uniform critical fluctuation size  $q^*$  by azimuthally averaging is a significant simplification (which clearly fails at the top right of the blue tear drop depicted in Figure 7). We have checked that for parameter values which exhibit

a less circular basin boundary the approximation of the mean switching times becomes worse.

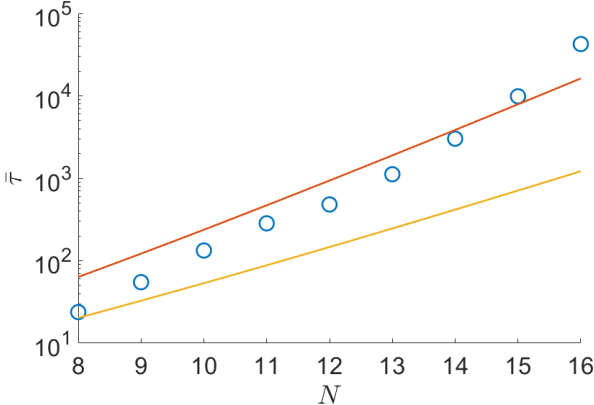


FIG. 18: Comparison of the mean switching time  $\bar{\tau}$  for different system sizes  $N$ , obtained from a long-time simulations of the full two-population KS model (1)–(2) (blue circles) and from the analytical expressions (40) and (43) based on solving Kramers problem using our reduced stochastic model. We show the result of the Kramers problem for  $q^* = 0.386$  (orange line) which was estimated from the full two-population KS model (1)–(2) (cf. Figure 7), and for  $q^* = 0.339$  (yellow line) which was estimated from the reduced deterministic mean-field model (26) (cf. Figures 9 and 10). Equation parameters are as in Figure 1.

## VII. SUMMARY AND OUTLOOK

We have shown that a deterministic two-population Kuramoto-Sakaguchi model can exhibit switching of chimera states whereby the two populations switch between a synchronised and desynchronised state in a seemingly random way. The switching events were shown to be uncorrelated events and to follow a Poisson distribution. The average time between switches was shown to increase exponentially with the system size  $N$  and hence switching constitutes a finite-size effect. As such, the effective stochastic behaviour cannot be described by the standard techniques valid in the thermodynamic limit. We evoked the central limit theorem to describe the fluctuations around the mean behaviour and employed the stochastic modelling framework from Yue and Gottwald<sup>51</sup>. The effective reduced stochastic model captures the statistics of both, the synchronised cluster and the switching of this cluster into a desynchronised state. Using mean-field theory we obtained an approximation of the critical size of finite-size fluctuations required to induce chimera switching. Our model produces relatively accurate predictions for the rate at which switching events become less frequent with increasing system size.

For illustration purposes, we have presented results for

a single set of parameters. We present in Appendix C further results for a different set of parameters to show the robustness of our approach.

Our approach here is entirely heuristic and relies on numerically fitting an Ornstein-Uhlenbeck process to the observed statistics of the fluctuations. It would be interesting to see if the approximation of the OU process can at least be formally justified. It was argued that the approximation of  $Z$  is related to a trigonometric approximation of Gaussian processes, where instead of trigonometric functions, the near-periodic solutions of the desynchronised oscillators are used<sup>51</sup>. This suggests a theoretical avenue to put the heuristic method employed here on a more rigorous footing.

The  $N$ -dimensional reduced stochastic model is still relatively high-dimensional and it would be interesting to see if it can be further reduced. Since the system-size  $N$  is not sufficiently large to allow for mean-field theory to capture the finite-size induced switching we need to resort to methods which are valid for finite-size systems such as the method of collective coordinates<sup>22,56–59</sup> which has already been shown to work for stochastically driven Kuramoto models<sup>23</sup>. This would allow for a straightforward calculation of the Kramers problem to calculate the transition probabilities describing switching chimeras.

In Section IV we saw that for certain parameters, i.e.,  $K = 85$ ,  $\kappa = 55$  and  $\lambda = \pi/2 - 0.09$ , the chimera state forms around a limit cycle. In this case, the interaction term  $Z$  will not be a centred Gaussian, but its density will be supported on a circular stripe. It is planned for further research to extend our stochastic modelling framework to this case of a breathing chimera.

## ACKNOWLEDGMENTS

GAG would like to acknowledge Wenqi Yue, from whom we learned about this interesting phenomenon.

- <sup>1</sup>S. M. Crook, G. B. Ermentrout, M. C. Vanier, and J. M. Bower, “The role of axonal delay in the synchronization of networks of coupled cortical oscillators,” *Journal of Computational Neuroscience* **4**, 161–172 (1997).
- <sup>2</sup>J. H. Sheeba, A. Stefanovska, and P. V. E. McClintock, “Neuronal synchrony during anesthesia: A thalamocortical model,” *Biophysical Journal* **95**, 2722–2727 (2008).
- <sup>3</sup>D. Bhowmik and M. Shanahan, “How well do oscillator models capture the behaviour of biological neurons?” in *The 2012 International Joint Conference on Neural Networks (IJCNN)* (2012) pp. 1–8.
- <sup>4</sup>R. Mirolo and S. Strogatz, “Synchronization of pulse-coupled biological oscillators,” *SIAM Journal on Applied Mathematics* **50**, 1645–1662 (1990), <https://doi.org/10.1137/0150098>.
- <sup>5</sup>G. Filatrella, A. H. Nielsen, and N. F. Pedersen, “Analysis of a power grid using a Kuramoto-like model,” *Eur. Phys. J. B* **61**, 485–491 (2008).
- <sup>6</sup>T. Nishikawa and A. E. Motter, “Comparative analysis of existing models for power-grid synchronization,” *New J. Phys.* **17** (2015), 10.1088/1367-2630/17/1/015012.
- <sup>7</sup>S. Watanabe and S. H. Strogatz, “Constants of motion for superconducting Josephson arrays,” *Physica D* **74**, 197 – 253 (1994).

- <sup>8</sup>K. Wiesenfeld, P. Colet, and S. H. Strogatz, "Frequency locking in Josephson arrays: Connection with the Kuramoto model," *Phys. Rev. E* **57**, 1563–1569 (1998).
- <sup>9</sup>Y. Kuramoto, *Chemical Oscillations, Waves, and Turbulence*, Springer Series in Synergetics, Vol. 19 (Springer-Verlag, Berlin, 1984) pp. viii+156.
- <sup>10</sup>H. Sakaguchi and Y. Kuramoto, "A soluble active rotator model showing phase transitions via mutual entrainment," *Prog. Theor. Phys.* **76**, 576–581 (1986).
- <sup>11</sup>S. H. Strogatz, "From Kuramoto to Crawford: Exploring the onset of synchronization in populations of coupled oscillators," *Physica D* **143**, 1–20 (2000).
- <sup>12</sup>A. Pikovsky, M. Rosenblum, and J. Kurths, *Synchronization: A Universal Concept in Nonlinear Sciences* (Cambridge University Press, Cambridge, 2001).
- <sup>13</sup>J. A. Acebrón, L. L. Bonilla, C. J. Pérez Vicente, F. Ritort, and R. Spigler, "The Kuramoto model: A simple paradigm for synchronization phenomena," *Rev. Mod. Phys.* **77**, 137–185 (2005).
- <sup>14</sup>G. V. Osipov, J. Kurths, and C. Zhou, *Synchronization in Oscillatory Networks*, Springer Series in Synergetics (Springer, Berlin, 2007) p. 37c.
- <sup>15</sup>A. Arenas, A. Diaz-Guilera, J. Kurths, Y. Moreno, and C. Zhou, "Synchronization in complex networks," *Phys. Rep.* **469**, 93–153 (2008).
- <sup>16</sup>F. Dörfler and F. Bullo, "Synchronization in complex networks of phase oscillators: A survey," *Automatica* **50**, 1539 – 1564 (2014).
- <sup>17</sup>F. A. Rodrigues, T. K. D. Peron, P. Ji, and J. Kurths, "The Kuramoto model in complex networks," *Phys. Rep.* **610**, 1 – 98 (2016).
- <sup>18</sup>E. Ott and T. M. Antonsen, "Low dimensional behavior of large systems of globally coupled oscillators," *Chaos* **18**, 037113, 6 (2008).
- <sup>19</sup>M. G. Delgadino, R. S. Gvalani, and G. A. Pavliotis, "On the diffusive-mean field limit for weakly interacting diffusions exhibiting phase transitions," *Arch. Ration. Mech. Anal.* **241**, 91–148 (2021).
- <sup>20</sup>G. Giacomin and C. Poquet, "Noise, interaction, nonlinear dynamics and the origin of rhythmic behaviors," *Braz. J. Probab. Stat.* **29**, 460–493 (2015).
- <sup>21</sup>E. Luçon, "Large population asymptotics for interacting diffusions in a quenched random environment," in *From particle systems to partial differential equations. II*, Springer Proc. Math. Stat., Vol. 129 (Springer, Cham, 2015) pp. 231–251.
- <sup>22</sup>G. A. Gottwald, "Model reduction for networks of coupled oscillators," *Chaos* **25**, 053111, 12 (2015).
- <sup>23</sup>G. A. Gottwald, "Finite-size effects in a stochastic Kuramoto model," *Chaos* **27**, 101103 (2017).
- <sup>24</sup>E. J. Hildebrand, M. A. Buice, and C. C. Chow, "Kinetic theory of coupled oscillators," *Phys. Rev. Lett.* **98**, 054101 (2007).
- <sup>25</sup>M. A. Buice and C. C. Chow, "Correlations, fluctuations, and stability of a finite-size network of coupled oscillators," *Phys. Rev. E* **76**, 031118 (2007).
- <sup>26</sup>H. Hong, M. Ha, and H. Park, "Finite-size scaling in complex networks," *Phys. Rev. Lett.* **98**, 258701 (2007).
- <sup>27</sup>L.-H. Tang, "To synchronize or not to synchronize, that is the question: finite-size scaling and fluctuation effects in the Kuramoto model," *Journal of Statistical Mechanics: Theory and Experiment* **2011**, P01034 (2011).
- <sup>28</sup>K. Okuda and Y. Kuramoto, "Mutual entrainment between populations of coupled oscillators," *Progr. Theoret. Phys.* **86**, 1159–1176 (1991).
- <sup>29</sup>E. Montbrió, J. Kurths, and B. Blasius, "Synchronization of two interacting populations of oscillators," *Phys. Rev. E* **70**, 056125 (2004).
- <sup>30</sup>Y. Kuramoto and D. Battogtokh, "Coexistence of coherence and incoherence in nonlocally coupled phase oscillators," *Nonlinear Phenom. Complex Syst.* **5**, 380?385 (2002).
- <sup>31</sup>O. E. Omel'chenko, Y. L. Maistrenko, and P. A. Tass, "Chimera states: The natural link between coherence and incoherence," *Phys. Rev. Lett.* **100**, 044105 (2008).
- <sup>32</sup>O. E. Omel'chenko, M. Wolfrum, and Y. L. Maistrenko, "Chimera states as chaotic spatiotemporal patterns," *Phys. Rev. E* **81**, 065201 (2010).
- <sup>33</sup>O. E. Omel'chenko, "The mathematics behind chimera states," *Nonlinearity* **31**, R121 (2018).
- <sup>34</sup>M. J. Panaggio, D. M. Abrams, P. Ashwin, and C. R. Laing, "Chimera states in networks of phase oscillators: The case of two small populations," *Phys. Rev. E* **93**, 012218 (2016).
- <sup>35</sup>O. Burylko, E. A. Martens, and C. Bick, "Symmetry breaking yields chimeras in two small populations of Kuramoto-type oscillators," *Chaos: An Interdisciplinary Journal of Nonlinear Science* **32**, 093109 (2022).
- <sup>36</sup>D. M. Abrams, R. Mirolo, S. H. Strogatz, and D. A. Wiley, "Solvable model for chimera states of coupled oscillators," *Physical Review Letters* **101** (2008), 10.1103/physrevlett.101.084103.
- <sup>37</sup>C. R. Laing, "Chimera states in heterogeneous networks," *Chaos: An Interdisciplinary Journal of Nonlinear Science* **19** (2009), 10.1063/1.3068353.
- <sup>38</sup>E. A. Martens, C. Bick, and M. J. Panaggio, "Chimera states in two populations with heterogeneous phase-lag," *Chaos: An Interdisciplinary Journal of Nonlinear Science* **26** (2016), 10.1063/1.4958930.
- <sup>39</sup>R. Ma, J. Wang, and Z. Liu, "Robust features of chimera states and the implementation of alternating chimera states," *Europhysics Letters* **91**, 40006 (2010).
- <sup>40</sup>C. R. Laing, "Disorder-induced dynamics in a pair of coupled heterogeneous phase oscillator networks," *Chaos: An Interdisciplinary Journal of Nonlinear Science* **22**, 043104 (2012).
- <sup>41</sup>A. Buscarino, M. Frasca, L. V. Gambuzza, and P. Hövel, "Chimera states in time-varying complex networks," *Phys. Rev. E* **91**, 022817 (2015).
- <sup>42</sup>N. Semenova, A. Zakharova, V. Anishchenko, and E. Schöll, "Coherence-resonance chimeras in a network of excitable elements," *Phys. Rev. Lett.* **117**, 014102 (2016).
- <sup>43</sup>Y. Zhang, Z. G. Nicolaou, J. D. Hart, R. Roy, and A. E. Motter, "Critical switching in globally attractive chimeras," *Phys. Rev. X* **10**, 011044 (2020).
- <sup>44</sup>C. Bick, "Heteroclinic switching between chimeras," *Phys. Rev. E* **97**, 050201 (2018).
- <sup>45</sup>C. Bick, "Heteroclinic dynamics of localized frequency synchrony: Heteroclinic cycles for small populations," *Journal of Nonlinear Science* **29**, 2547–2570 (2019).
- <sup>46</sup>C. Bick and A. Lohse, "Heteroclinic dynamics of localized frequency synchrony: Stability of heteroclinic cycles and networks," *Journal of Nonlinear Science* **29**, 2571–2600 (2019).
- <sup>47</sup>P. Ebrahimbzadeh, M. Schiek, P. Jaros, T. Kapitaniak, S. van Waasen, and Y. Maistrenko, "Minimal chimera states in phase-lag coupled mechanical oscillators," *The European Physical Journal Special Topics* **229**, 2205–2214 (2020).
- <sup>48</sup>R. J. Goldschmidt, A. Pikovsky, and A. Politi, "Blinking chimeras in globally coupled rotators," *Chaos: An Interdisciplinary Journal of Nonlinear Science* **29**, 071101 (2019).
- <sup>49</sup>S. Brezetsky, P. Jaros, R. Levchenko, T. Kapitaniak, and Y. Maistrenko, "Chimera complexity," *Phys. Rev. E* **103**, L050204 (2021).
- <sup>50</sup>S. Lee and K. Krischer, "Heteroclinic switching between chimeras in a ring of six oscillator populations," *Chaos: An Interdisciplinary Journal of Nonlinear Science* **33**, 063120 (2023).
- <sup>51</sup>W. Yue and G. A. Gottwald, "A stochastic approximation for the finite-size Kuramoto-Sakaguchi model," *Physica D: Nonlinear Phenomena* **468**, 134292 (2024).
- <sup>52</sup>H. Kramers, "Brownian motion in a field of force and the diffusion model of chemical reactions," *Physica* **7**, 284–304 (1940).
- <sup>53</sup>C. Bick, M. Goodfellow, C. R. Laing, and E. A. Martens, "Understanding the dynamics of biological and neural oscillator networks through exact mean-field reductions: a review," *J. Math. Neurosc.* **10**, 9 (2020).
- <sup>54</sup>F. Peter and A. Pikovsky, "Transition to collective oscillations in finite Kuramoto ensembles," *Phys. Rev. E* **97**, 032310 (2018).
- <sup>55</sup>J. Fialkowski, S. Yanchuk, I. M. Sokolov, E. Schöll, G. A.

- Gottwald, and R. Berner, "Heterogeneous nucleation in finite-size adaptive dynamical networks," *Phys. Rev. Lett.* **130**, 067402 (2023).
- <sup>56</sup>E. J. Hancock and G. A. Gottwald, "Model reduction for Kuramoto models with complex topologies," *Phys. Rev. E* **98**, 012307 (2018).
- <sup>57</sup>L. D. Smith and G. A. Gottwald, "Chaos in networks of coupled oscillators with multimodal natural frequency distributions," *Chaos* **29**, 093127 (2019).
- <sup>58</sup>L. D. Smith and G. A. Gottwald, "Model reduction for the collective dynamics of globally coupled oscillators: From finite networks to the thermodynamic limit," *Chaos: An Interdisciplinary Journal of Nonlinear Science* **30** (2020), 10.1063/5.0009790.
- <sup>59</sup>W. Yue, L. D. Smith, and G. A. Gottwald, "Model reduction for the Kuramoto-Sakaguchi model: The importance of non-trained rogue oscillators," *Phys. Rev. E* **101**, 062213 (2020).
- <sup>60</sup>P. Vatiwutipong and N. Phewchean, "Alternative way to derive the distribution of the multivariate Ornstein-Uhlenbeck process," *Advances in Difference Equations* **2019**, 276 (2019).
- <sup>61</sup>M. Sachs, B. Leimkuhler, and V. Danos, "Langevin dynamics with variable coefficients and nonconservative forces: From stationary states to numerical methods," *Entropy* **19** (2017), 10.3390/e19120647.

## Appendix A: Justification for the approximations (24)

We present here a more formal justification for the approximations (24) used to close the mean-field dynamics (20). We begin by expressing

$$z_\alpha^{(2,0)} - z_\alpha^2 = \text{var}(\text{Re}(e^{i\theta^{(\alpha)}})) - \text{var}(\text{Im}(e^{i\theta^{(\alpha)}})) + 2i \text{cov}(\text{Re}(e^{i\theta^{(\alpha)}}), \text{Im}(e^{i\theta^{(\alpha)}})), \quad (\text{A1})$$

where  $\text{var}$  and  $\text{cov}$  denote the empirical variance and covariance across  $P_\alpha$ , respectively, which is readily bounded by

$$|z_\alpha^{(2,0)} - z_\alpha^2| \leq \text{var}(\text{Re}(e^{i\theta_j^{(\alpha)}})) + \text{var}(\text{Im}(e^{i\theta_j^{(\alpha)}})) = 1 - r_\alpha^2. \quad (\text{A2})$$

For the synchronised population with  $\alpha = 1$  we have  $r_1 \approx 1$  which immediately yields the first approximation in (24). For  $\alpha = 2$ , the bound (A2) is less sharp.

To approximate  $z_\alpha^{(1,1)}$ , we expand

$$\begin{aligned} z_\alpha^{(1,1)} &= \frac{1}{N} \sum_{j=1}^N \omega_j^{(\alpha)} e^{i\theta_j^{(\alpha)}} \\ &= \langle \omega_j^{(\alpha)} \rangle_{j \in P_\alpha} \left( \frac{1}{N} \sum_{j=1}^N e^{i\theta_j^{(\alpha)}} \right) \\ &\quad + \text{cov}(\omega_j^{(\alpha)}, \text{Re}(e^{i\theta_j^{(\alpha)}})) \\ &\quad + i \text{cov}(\omega_j^{(\alpha)}, \text{Im}(e^{i\theta_j^{(\alpha)}})). \end{aligned} \quad (\text{A3})$$

The native frequencies  $\omega_j^{(\alpha)}$  are drawn from a Gaussian distribution  $\mathcal{N}(0, \sigma_\omega^2)$  and hence (A3) can be bounded by

$$\begin{aligned} |z_\alpha^{(1,1)} - 0| &\lesssim \sigma_\omega \sqrt{\text{var}(\text{Re}(e^{i\theta_j^{(\alpha)}})) + \text{var}(\text{Im}(e^{i\theta_j^{(\alpha)}}))} \\ &= \sigma_\omega \sqrt{1 - r_\alpha^2}. \end{aligned} \quad (\text{A4})$$

Again for the synchronised population with  $\alpha = 1$  and  $r_1 \approx 1$  the second approximation in (24) follows immediately.

A necessary condition of the validity of the approximations (24) is that they need to be consistent with the dynamics (23) in the sense that if they are satisfied at any time, they remain satisfied for all times. Unfortunately, this is not the case as can be readily seen from (23), which involves higher moments. However, if initially we require the stronger conditions

$$\begin{aligned} z_\alpha^{(m,n)} &= z_\alpha^m, \quad \text{for } n = 0, \\ z_\alpha^{(m,n)} &= 0, \quad \text{for } n \neq 0, \end{aligned} \quad (\text{A5})$$

for  $\alpha = 1, 2$  and  $m, n \in \mathbb{N}$ , we can show that they remain satisfied if so at any time. We provide the motivation behind the assumptions (A5) in Appendix A 1. Note that for  $(m = 0, n = 0)$  and  $(m = 1, n = 0)$  the conditions are trivially satisfied, and  $(m = 2, n = 0)$  and  $(m = 1, n = 1)$  correspond to (24).

Using the unperturbed dynamics (20) the conditions (A5) imply that

$$\begin{aligned} \frac{d}{dt} z_\alpha^{(m,0)} &= \frac{d}{dt} z_\alpha^m \\ &= m \frac{1}{2} (v_\alpha z_\alpha^{m-1} - v_\alpha^* z_\alpha^{(2,0)} z_\alpha^{m-1}), \end{aligned} \quad (\text{A6})$$

for  $\alpha = 1, 2$ , and  $v_\alpha$  defined in (21). Since (A5) implies  $z_\alpha^{(m,0)} z_\alpha^{m'} = z_\alpha^{(m+m',0)}$  for all  $m, m' \in \mathbb{N}$ , (A6) simplifies to

$$\frac{d}{dt} z_\alpha^{(m,n)} = m (i z_\alpha^{(m,n+1)} + \frac{1}{2} (v_\alpha z_\alpha^{(m-1,n)} - v_\alpha^* z_\alpha^{(m+1,n)})), \quad (\text{A7})$$

for  $n = 0$  and  $\alpha = 1, 2$ . Note that (A7) is trivially valid for  $n \neq 0$ , and corresponds to the unperturbed dynamics (23). This implies that if the conditions (A5) hold true for any point in time, then they must be true for all times. We remark that there is an infinite family of conditions with this self-consistency property, which we describe in Appendix A 2.

### 1. Motivation for conditions (A5)

For small variance of the native frequencies,  $\sigma_\omega^2$ , we approximate  $\omega_j^{(\alpha)} \approx \bar{\omega}^{(\alpha)}$ , where  $\bar{\omega}^{(\alpha)}$  is the mean of the native frequencies of population  $P_\alpha$ . Assuming further that the dynamics is near a stable equilibrium at the thermodynamic limit, we approximate (22) as

$$z_\alpha^{(m,n)} \approx (\bar{\omega}^{(\alpha)})^n \langle e^{im\theta^{(\alpha)}} \rangle. \quad (\text{A8})$$

For entrained oscillators, it is readily shown that

$$\langle e^{im\theta^{(\alpha)}} \rangle = (\langle e^{im\theta^{(\alpha)}} \rangle)^m. \quad (\text{A9})$$

Non-entrained oscillators are distributed according to the stationary distribution (14), and we can write

$$\begin{aligned}\langle e^{im\theta^{(\alpha)}} \rangle &= \int_{-\pi}^{\pi} e^{im\theta} \rho^{(\alpha)}(\theta) d\theta \\ &= \frac{\int_{-\pi}^{\pi} \frac{e^{im\theta}}{\nu^{(\alpha)}} d\theta}{\int_{-\pi}^{\pi} \frac{1}{\nu^{(\alpha)}} d\theta} \\ &= \int_{-\pi}^{\pi} \frac{e^{im\theta}}{2\pi} \frac{\sqrt{(\bar{\omega}^{(\alpha)} - \Omega)^2 - |v_{\alpha}|^2}}{\bar{\omega}^{(\alpha)} - \Omega + \text{Im}(v_{\alpha} e^{-i\theta})} d\theta \quad (\text{A10})\end{aligned}$$

Introducing for ease of exposition

$$\begin{aligned}p &= \frac{\bar{\omega}^{(\alpha)} - \Omega}{|v_{\alpha}|} - \sqrt{\frac{\bar{\omega}^{(\alpha)} - \Omega}{|v_{\alpha}|} - 1} \sqrt{\frac{\bar{\omega}^{(\alpha)} - \Omega}{|v_{\alpha}|} + 1}, \\ v &= i \frac{v_{\alpha}}{|v_{\alpha}|}, \quad (\text{A11})\end{aligned}$$

we write

$$\begin{aligned}\langle e^{im\theta^{(\alpha)}} \rangle &= \int_{-\pi}^{\pi} \frac{e^{im\theta}}{2\pi} \frac{1-p^2}{1+p^2-2p\text{Re}(ve^{-i\theta})} d\theta \\ &= \int_{-\pi}^{\pi} \frac{e^{im\theta}}{2\pi} \frac{1-p^2}{1+p^2-p\left(\frac{v}{e^{i\theta}}+\frac{e^{i\theta}}{v}\right)} d\theta \\ &= \int_{-\pi}^{\pi} \frac{e^{im\theta}}{2\pi} \left(1+\frac{p\frac{v}{e^{i\theta}}}{1-p\frac{v}{e^{i\theta}}}+\frac{p\frac{e^{i\theta}}{v}}{1-p\frac{e^{i\theta}}{v}}\right) d\theta \\ &= \int_{-\pi}^{\pi} \frac{e^{im\theta}}{2\pi} \sum_{n=-\infty}^{\infty} p^{|n|} \left(\frac{v}{e^{i\theta}}\right)^n d\theta \\ &= \sum_{n=-\infty}^{\infty} p^{|n|} v^n \int_{-\pi}^{\pi} \frac{e^{i(m-n)\theta}}{2\pi} d\theta \\ &= p^{|m|} v^m. \quad (\text{A12})\end{aligned}$$

Therefore, we are left with the approximation of

$$z_{\alpha}^{(m,n)} \approx (\bar{\omega}^{(\alpha)})^n z_{\alpha}^m. \quad (\text{A13})$$

With  $\bar{\omega} = 0$  the approximations (A5) immediately follow.

## 2. Self-consistent approximations for $z_{\alpha}^{(m,n)}$

Here we derive a more general set of approximations for  $z_{\alpha}^{(m,n)}$  which satisfies the set of self-consistency conditions (A5). We restrict the approximations to be of the form

$$z_{\alpha}^{(m,n)} = c^n e^{mi\psi_{\alpha}} f_m(r_{\alpha}), \quad (\text{A14})$$

where  $f_m$  is an unknown function to be determined. Special cases are  $f_0(r_{\alpha}) = 1$  and  $f_1(r_{\alpha}) = r_{\alpha}$ .

$$\begin{aligned}\frac{d}{dt} z_{\alpha}^{(m,n)} &= c^n e^{mi\psi_{\alpha}} (f'_m(r_{\alpha}) \frac{dr_{\alpha}}{dt} + i m f_m(r_{\alpha}) \frac{d\psi_{\alpha}}{dt}) \\ &= c^n e^{mi\psi_{\alpha}} \left( f'_m(r_{\alpha}) \frac{(1-f_2(r_{\alpha})) \text{Re}(v_{\alpha} e^{-i\psi_{\alpha}})}{2} \right. \\ &\quad \left. + i m f_m(r_{\alpha}) (c + \frac{(1+f_2(r_{\alpha})) \text{Im}(v_{\alpha} e^{-i\psi_{\alpha}})}{2r_{\alpha}}) \right). \quad (\text{A15})\end{aligned}$$

Equating (A15) with (23) determines a recursive relationship for  $f_m$  with

$$f_{m+1}(r_{\alpha}) = f_m(r_{\alpha}) \frac{1+f_2(r_{\alpha})}{r_{\alpha}} - f_{m-1}(r_{\alpha}), \quad (\text{A16})$$

$$f'_m(r_{\alpha}) = m \frac{f_{m-1}(r_{\alpha}) - f_{m+1}(r_{\alpha})}{1-f_2(r_{\alpha})}. \quad (\text{A17})$$

Additionally, we remark that (A17) holding true for  $m = 2$ , and (A16) holding true for all  $m$ , implies that (A17) holds true for all  $m$ . This means that to find a valid set of functions  $f_m$ , we must only find some  $f_2$  that satisfies

$$f'_2(r_{\alpha}) = 2 \frac{2r_{\alpha} - f_2(r_{\alpha}) \frac{1+f_2(r_{\alpha})}{r_{\alpha}}}{1-f_2(r_{\alpha})} - 1. \quad (\text{A18})$$

For  $m > 2$ ,  $f_m$  is determined recursively from  $f_{0,1,2}(r_{\alpha})$ . We find that (A18) is satisfied by the family of solutions to the equations

$$f_2(r_{\alpha}) = 2r_{\alpha} \frac{r_{\alpha}(4-g^2) + g\sqrt{4-r_{\alpha}^2(4-g^2)}}{4} - 1, \quad (\text{A19})$$

for any  $g \in \mathbb{R}$ . For  $g \rightarrow \infty$ , for example, we obtain  $f_2(r) = r^2$ . Substituting  $f_m$  into (A14) we find

$$\begin{aligned}z_{\alpha}^{(m,n)} &= \lim_{g_0 \rightarrow g} c^n e^{mi\psi_{\alpha}} \sum_{s=-1,1} \left( \frac{1}{2} + s \frac{r_{\alpha} - C_{\alpha}(g_0)}{2\sqrt{C_{\alpha}(g_0)^2 - 1}} \right) \\ &\quad \left( C_{\alpha}(g_0) + s\sqrt{C_{\alpha}(g_0)^2 - 1} \right)^m \quad (\text{A20})\end{aligned}$$

for any constants  $c \in \mathbb{C}$ ,  $g \in \mathbb{R} \cup \{\infty\}$  and with

$$C_{\alpha}(g_0) = \frac{r_{\alpha}(4-g_0^2) + g_0\sqrt{4-r_{\alpha}^2(4-g_0^2)}}{4}. \quad (\text{A21})$$

Note that for  $c = 0$  and  $g = \infty$  (A20) yields condition (A5) with  $z_{\alpha}^{(m,n)} = 0^n z_{\alpha}^m$ .

## Appendix B: Numerical integrator for the OU process

Consider a general  $k$ -dimensional stochastic OU process

$$d\zeta = -\Gamma\zeta dt + \Sigma dW_t, \quad (\text{B1})$$

where  $\Gamma \in \mathbb{R}^{k \times k}$  and  $\Sigma \in \mathbb{R}^{k \times k}$  are the drift and diffusion matrices, respectively, and  $W_t$  is a  $k$ -dimensional Wiener process.

To numerically integrate the multivariate OU process (B1) with a fixed time step  $\Delta t$ , we employ a modified Euler-Maruyama scheme

$$\zeta_{n+1} = \zeta_n - \hat{\Gamma} \zeta_n \Delta t + \hat{\Sigma} \Delta W_n, \quad (\text{B2})$$

with  $\Delta W \sim \mathcal{N}(0, \Delta t \mathbf{I})$  and

$$\hat{\Gamma} = \frac{\mathbf{I} - e^{-\Gamma \Delta t}}{\Delta t} \quad (\text{B3})$$

and

$$\hat{\Sigma} = \sqrt{\frac{\int_0^{\Delta t} \exp(-\Gamma s) \Sigma \Sigma^\top \exp(-\Gamma^\top s) ds}{\Delta t}}. \quad (\text{B4})$$

Note that  $\lim_{\Delta t \rightarrow 0} \hat{\Gamma} = \Gamma$  and  $\lim_{\Delta t \rightarrow 0} \hat{\Sigma} = \Sigma$ . The modified Euler-Maruyama scheme (B2) has the desirable property that it preserves the true transition density  $\rho(\zeta_{n+1} | \zeta_n)$  of the underlying process (B1); see, for example,<sup>60</sup>.

The integral over the matrix exponential in (B4),

$$\int_0^t \exp(-\Gamma s) \Sigma \Sigma^\top \exp(-\Gamma^\top s) ds, \quad (\text{B5})$$

can be explicitly calculated for diagonalizable drift matrices  $\Gamma = V D V^{-1}$  with diagonal  $D$  as

$$\begin{aligned} & \int_0^t \exp(-\Gamma s) \Sigma \Sigma^\top \exp(-\Gamma^\top s) ds \\ &= \int_0^t \exp(-V D V^{-1} s) \Sigma \Sigma^\top \exp(-V^{-\top} D V^\top s) ds \\ &= V \left( \int_0^t \exp(-Ds) V^{-1} \Sigma \Sigma^\top V^{-\top} \exp(-Ds) ds \right) V^\top \\ &= V \left( V^{-1} \Sigma \Sigma^\top V^{-\top} \odot \int_0^t \exp_{\circ}(-(D\mathbf{1} + \mathbf{1}D)s) ds \right) V^\top \\ &= V (V^{-1} \Sigma \Sigma^\top V^{-\top} \oslash (D\mathbf{1} + \mathbf{1}D) \\ &\quad \odot (\mathbf{1} - \exp_{\circ}(-(D\mathbf{1} + \mathbf{1}D)t))) V^\top, \end{aligned} \quad (\text{B6})$$

where  $\odot$ ,  $\oslash$  and  $\exp_{\circ}$  denote Hadamard multiplication, division and exponentiation respectively, and  $\mathbf{1} \in \mathbb{R}^{k \times k}$  denotes a matrix consisting of 1s.

In the special case where drift and diffusion matrices are in the form (33)-(34), (B6) simplifies to

$$\begin{aligned} & \int_0^t \exp(-\Gamma s) \Sigma \Sigma^\top \exp(-\Gamma^\top s) ds \\ &= \frac{\sigma^2}{2 \operatorname{Re}(\gamma)} \exp(-2 \operatorname{Re}(\gamma)) \mathbf{I}. \end{aligned} \quad (\text{B7})$$

We remark that for more general cases the analytical formula for the variance can be costly to compute in high dimensions, and one may be well advised to employ a naive approach of repeated Euler-Maruyama steps<sup>61</sup>.

## Appendix C: Additional numerical results

To show that our stochastic modelling framework is generally valid, we present results for a different choice of parameters with  $K = 85$ ,  $\kappa = 55$  and  $\lambda = \pi/2 - 0.09$ . For these parameters we obtain  $\langle Z \rangle = 0.689 + 0.131i$  from the mean-field theory. Fitting the covariance function by minimising the cost function (35) from  $t_{\min} = 0.5$  to  $t_{\max} = 1$  yields  $\gamma = 1.918 - 18.05i$  and  $\sigma = 0.335$ .

We show in Figures 19–23 that our stochastically driven model (29)–(30) reproduces the statistics of the order parameter and the phases very well. The case of a small network with  $N = 8$  is less well approximated. Figure 23 shows the mean rotation frequency  $\bar{\nu}_i$  for various values of  $N$ . We used the mean-field result for  $\langle Z \rangle$  in the reduced stochastic model (29)–(30). We remark that if we used the empirical mean estimated from simulations of the two-population KS model (1)–(2) for each value of  $N$  the mean rotation frequencies are as accurate as those shown in Figure 17. Figure 24 shows that the azimuthally averaged equation for the fluctuations is capable to provide good estimates of the mean switching time using the Kramers problem solution (43).

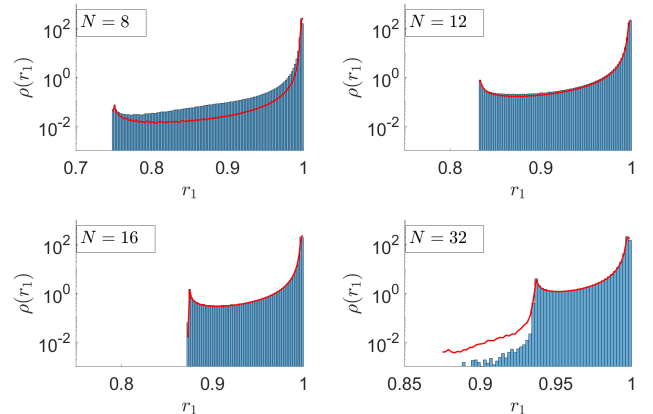


FIG. 19: Comparison of the empirical histograms for the order parameter  $r_1$  of the synchronised population obtained from a single trajectory of the full two-population KS model (1)–(2) (blue histogram) and from the reduced stochastic model (29)–(30) (red line) for  $N = 8, 12, 16$  and  $32$ . A log scale has been applied to the  $y$ -axis. Equation parameters are as  $K = 85$ ,  $\kappa = 55$  and  $\lambda = \pi/2 - 0.09$ .

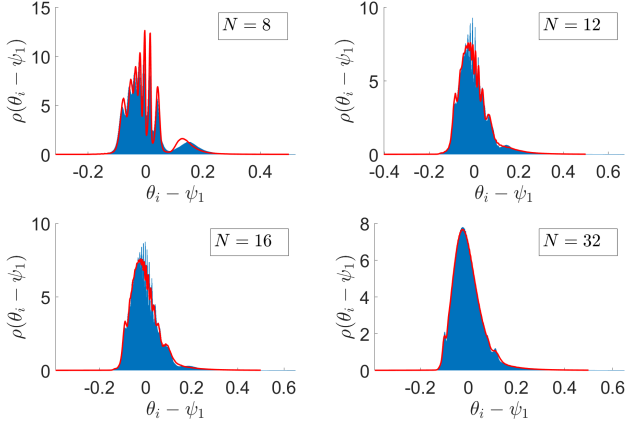


FIG. 20: Comparison of the empirical histograms for the fluctuations of the synchronised phases around their mean,  $\theta_i - \psi_1$ , obtained from a single trajectory of the full two-population KS model (1)–(2) (blue histogram) and of the reduced stochastic model (29)–(30) (red line) for  $N = 8, 12, 16$  and  $32$ . Equation parameters are as in Figure 19.

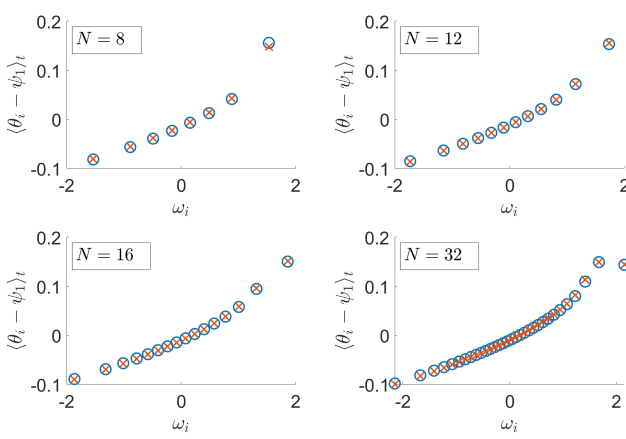


FIG. 21: Mean of the fluctuations of the synchronised phases around their mean,  $\theta_i - \psi_1$ , as a function of their native frequencies  $\omega_i$  for the full two-population KS model (1)–(2) (blue circles) and for the reduced stochastic model (29)–(30) (red crosses) for  $N = 8, 12, 16$  and  $32$ . Equation parameters are as in Figure 19.

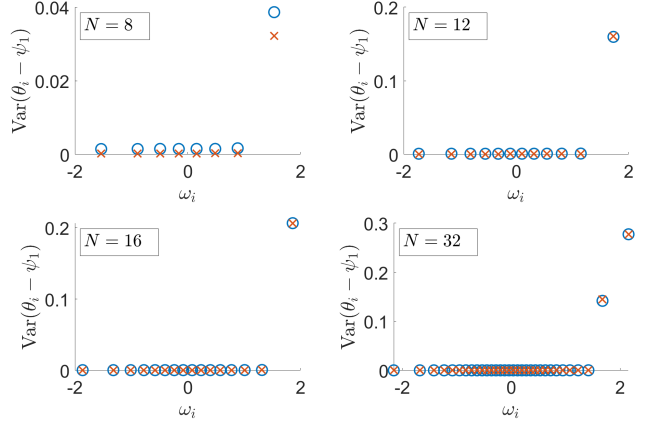


FIG. 22: Variance of the fluctuations of the synchronised phases around their mean,  $\theta_i - \psi_1$ , as a function of their native frequencies  $\omega_i$  for the full two-population KS model (1)–(2) (blue circles) and for the reduced stochastic model (29)–(30) (red crosses) for  $N = 8, 12, 16$  and  $32$ . Equation parameters are as in Figure 19.

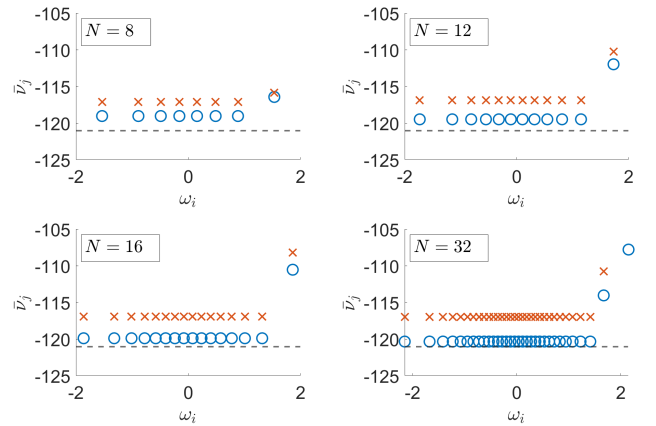


FIG. 23: Mean rotation frequency  $\bar{v}_i$  of the synchronised oscillators as a function of their native frequencies  $\omega_i$  for the full two-population KS model (1)–(2) (blue circles) and for the reduced stochastic model (28)–(29) (red crosses) for  $N = 8, 12, 16$  and  $32$ . The dashed lines denote the mean frequency  $\Omega$  as calculated from the self-consistency relations (17)–(18) of the mean-field theory. Equation parameters are as in Figure 19.

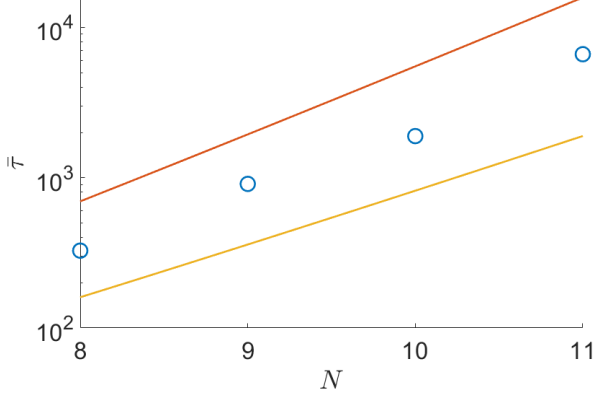


FIG. 24: Comparison of the mean switching time  $\bar{\tau}$  for different system sizes  $N$ , obtained from a long-time simulations of the full two-population KS model (1)–(2) (blue circles) and from the analytical expression (40) and (43) based on solving Kramers problem using our reduced stochastic model. We show the result of the Kramers problem for  $q^* = 0.261$  (orange line) which was estimated from the full two-population KS model (1)–(2), and for  $q^* = 0.236$  (yellow line) which was estimated from the reduced deterministic mean-field model (26). Equation parameters are as in Figure 19.